RATE-LIMITING STEPS ON FUEL-CELL ELECTRODES

TECHNICAL DOCUMENTARY REPORT ASD-TDR-63-118

JANUARY 1963

FLIGHT ACCESSORIES LABORATORY
AERONAUTICAL SYSTEMS DIVISION
AIR FORCE SYSTEMS COMMAND
WRIGHT-PATTERSON AIR FORCE BASE, OHIO

Project No. 8173, Task No. 817306

(Prepared under Contract No. AF 33(616)-7624
by Massachusetts Institute of Technology,
Research Laboratory of Electronics,
Energy Conversion Group,
Cambridge, Massachusetts.
Author: Adrian R. Reti)

NOTICES

When Government drawings, specifications, or other data are used for any purpose other than in connection with a definitely related Government procurement operation, the United States Government thereby incurs no responsibility nor any obligation whatsoever; and the fact that the Government may have formulated, furnished, or in any way supplied the said drawings, specifications, or other data, is not to be regarded by implication or otherwise as in any manner licensing the holder or any other person or corporation, or conveying any rights or permission to manufacture, use, or sell any patented invention that may in any way be related thereto.

Qualified requesters may obtain copies of this report from the Armed Services Technical Information Agency, (ASTIA), Arlington Hall Station, Arlington 12, Virginia.

This report has been released to the Office of Technical Services, U.S. Department of Commerce, Washington 25, D. C., for sale to the general public.

Copies of this report should not be returned to the Aeronautical Systems Division unless return is required by security considerations, contractual obligations, or notice on a specific document.

ASD TECHNICAL DOCUMENTARY REPORT 63-118

RATE-LIMITING STEPS ON FUEL-CELL ELECTRODES

Adrian R. Reti

Massachusetts Institute of Technology
Research Laboratory of Electronics
Energy Conversion Group
Cambridge, Massachusetts

January 1963

Flight Accessories Laboratory
Contract No. AF 33(616)-7624
Project No. 8173
Task No. 817306

AERONAUTICAL SYSTEMS DIVISION
AIR FORCE SYSTEMS COMMAND
UNITED STATES AIR FORCE
WRIGHT-PATTERSON AIR FORCE BASE, OHIO

FOREWORD

This report was initiated by the Flight Vehicle Power Branch, Flight Accessories Laboratory, Wright Air Development Division (now designated Aeronautical Systems Division), Wright-Patterson Air Force Base, Ohio. The work was done in the Research Laboratory of Electronics, Massachusetts Institute of Technology, Cambridge, Massachusetts, under Air Force Contract AF 33(616)-7624, Project Nr 8173, Task Nr 817306. Mr. Don R. Warnock was task engineer for the Flight Accessories Laboratory.

The research on which this report is based was performed by the author in partial fulfillment of the requirements for the degree of Doctor of Science, in the Department of Chemical Engineering, Massachusetts Institute of Technology, under the supervision of Professor H. P. Meissner.

Assistance provided by personnel of the Flight Accessories Laboratory, Aeronautical Systems Division, and by members of the staff of the Research Laboratory of Electronics, M. I. T., is gratefully acknowledged.

ABSTRACT

The purpose of this investigation was to identify and to study the step or steps that limit fuel cell electrode performance. The electrodes considered were the typical porous, gaseous diffusion type, and most of the effort was directed toward acquiring a more quantitative understanding of the effect of the different variables governing electrode performance.

Since it is necessary to be able to predict quantitatively both the mass transfer and the kinetic limitations in order to calculate electrode performances, an experimental program directed toward obtaining the necessary kinetic data for systems of interest was undertaken. An experimental system was devised by means of which the electrochemical kinetics could be studied over a wide current density range independently of mass transfer effects, on electrodes of known catalyst area. In the operating region where the effect of mass transfer became significant, it was possible quantitatively to assess its importance.

It was found that for all of the systems studied (O_2 and H_2O_2 electroreduction, H_2 and ethylene oxidation), for a particular catalyst-electrolyte system, the electrode performance could be described as a function of reactant concentration and current density only. The most significant finding in these electrochemical kinetic studies was that for both the O_2 and the H_2 systems, in the current density range of practical interest (10^{-2} to 10^{-4} amp/cm^2) the reactant chemisorption rate on the electrode surface plays an important role in governing the electrode potential, and makes it impossible to describe the electrode performance by a simple expression such as the Tafel equation.

Electrode performance calculations were made for the case of an oxygen electrode of idealized geometry, by using the experimentally obtained kinetic data and the known values of oxygen solubilities and diffusivities in liquid electrolytes. It was found that if the electrode geometrical parameters (pore size distribution, location, etc.) are properly chosen, electrode performances much superior to the ones thus far obtained by several investigators should be possible, showing that the potential performance of such types of electrodes has not yet been fully realized.

PUBLICATION REVIEW

The publication of this report does not constitute approval by the Air Force of the findings or conclusions contained herein. It is published for the exchange and stimulation of ideas.

TABLE OF CONTENTS

CONTENTS

LIST OF FIGURES

GLOSSARY

Symbol	Definition
A	Constant in adsorption equation
a	Constant in Tafel equation
B	Constant in adsorption equation
b	Constant in Tafel equation
C_D	Capacitance of dummy electrode D_{Ac} (Fd)
C_{DL}	Specific electrical double-layer capacitance (Fd/cm^2)
C_S	Capacitance of electrode system (Fd)
C_T	Capacitance of test electrode T (Fd)
c_o	Reactant concentration at gas-liquid interface (g. $moles/cm^3$)
c_s	Reactant concentration at electrode surface (g. $moles/cm^3$)
c_x	Reactant concentration at a distance x within a pore (g. $moles/cm^3$)
C_p	Specific heat (Btu/lb °F)
D	Macropore diameter (cm)
d	Micropore diameter (cm)
D_L	Liquid-phase diffusivity (cm^2/sec)
E_{act}	Measured electrode potential (volts)
E_{rev}	Reversible theoretical electrode potential (volts)
E_o	Standard electrode potential (volts)
F	Faraday's constant, 96,500 coulombs/gram equivalent
h	Heat-transfer coefficient (Btu/hr ft^2 °F)
I	Current (amps)
i_F	Face-area current density (amp/cm^2 electrode face area)
i_L	Limiting current density (amp/cm^2)
i_{Tot}	Total current density (amp/cm^2 of total electrode area)
i_S	Surface current density (amp/cm^2 of electrode active surface)
k	Thermal conductivity (Btu/hr ft °F)
k_L	Liquid-phase mass-transfer coefficient (cm/sec)

GLOSSARY (continued)

Symbol	Definition
L_R	"Active Length" of a macropore (cm)
N_{O_2}	Diffusional mass flux of oxygen (g. moles/sec cm^2)
N Re	Reynolds number (dimensionless)
n	Electrochemical transport number (Faradays/equivalent)
p	Partial pressure (atm)
q	Tortuosity path factor (dimensionless)
R	Gas constant, 1.986 calories/°K g. mole
R'	Resistance (ohms)
T	Temperature (°K)
t	Time (seconds)
U	Velocity (cm/sec)
V	Voltage (volts)
x	Axial distance from the gas-liquid interface in a pore (cm)
x_L	"Effective Length" of a micropore (cm)
ϵ	Fractional porosity (dimensionless)
θ	Fractional surface area coverage (dimensionless)
η	Electrode overvoltage = $E_{rev} - E_{act}$
ρ	Density (lb/ft^3)
ρ'	Resistivity (ohms-cm)
μ	Viscosity (lb/sec-ft)

I. INTRODUCTION*

The object of this investigation was to identify and investigate the rate-limiting step or steps in low temperature-aqueous electrolyte fuel-cell electrode systems, and to evaluate the performance obtainable from an electrode system specifically designed to remove or minimize these limitations.

Although the greatest part of this study has been concerned with the oxygen electrode, both experimentally and in performance calculations, we feel that many of the results apply to fuel-cell electrode systems in general, since the processes taking place at either oxidizer or fuel electrodes are quite similar in nature. The decision to place such an emphasis on the oxygen electrode was based on three considerations. First, the oxygen electrode is common to many fuel-cell systems, and its study contributes to the better understanding of all of these systems. Second, the oxygen electrode is the limiting electrode in many of these systems: that is, H_2-O_2, Sodium Amalgam-O_2, Hydrazine-O_2, and so forth, and knowledge and improvement of its performance is of capital importance. Third, the oxygen-electrode kinetics have been the subject of several investigations. Although these investigations do not provide the quantitative information required for performance calculations, they contribute to the understanding of the oxygen-electrode process in general, and they help to identify and to study the most important variables. The choice of a system the characteristics of which are already known made it possible to direct most of the effort toward previously identified problem areas, saving considerable time and effort at the initial stages of the project, as well as permitting the comparison of the results obtained with other experimental evidence during the interpretation of such results.

1.1 GENERAL BACKGROUND OF THE PROBLEM

a. The Gaseous Diffusion Electrode

The typical gaseous diffusion electrode used in most fuel-cell systems and considered in this work is shown in Fig. 1. The electrode consists of a highly interlinked porous system, with pore sizes and size distributions whose variation depends on the specific system. The liquid electrolyte is in contact with and penetrates, to a certain extent, one side of the electrode, while the reactant gas is able to penetrate and diffuse through the electrode pores from the other side. The position of the gas-liquid interface within the electrode is generally controlled by adjusting the gas pressure, modifying the average pore diameter within the electrode or changing the electrolyte-electrode contact angle by treatment of the internal surface with lyophylic materials.

*Manuscript released by the author, January 1963, for publication as an ASD Technical Documentary Report.

Several different processes take place at the electrode:

(i) The electrochemical reaction itself, in which molecules are either oxidized (lose electrons) or reduced (gain electrons). Since electrons must be transferred between the reacting molecules and the electrode surface, the electrochemical reaction must take place within the electrode material, or at its surface, since neither the gas nor the electrolyte phase is a good electron conductor. Similarly, since ions must be discharged or molecules must be ionized in this electrochemical reaction, the site where this reaction takes place must be in contact with the electrolyte, which is the only phase that is a good enough ionic conductor. These two restrictions indicate that the electrochemical reaction can take place exclusively at the electrode-electrolyte interface.

(ii) The reactants must somehow reach the electrode-electrolyte interface, and consequently must diffuse as necessary through the gas and liquid or solid phases within the electrodes.

(iii) The reaction products must leave the electrode-electrolyte interface, and must diffuse through the gas, liquid or solid phases too.

The restrictions to be kept in mind whenever the above-mentioned transport processes take place are:

(i) Molecules can diffuse through gases, liquids, and solids with different degrees of ease.

(ii) Electrons can only travel through electron conductors such as the electrode material (metals, carbon).

(iii) Ions can only travel through liquid electrolyte systems and ionic semiconductors (solid electrolytes).

In order to predict the current (reaction rate) obtainable from an electrode system, one must not only be able to predict the rate of the electrochemical reaction itself as a function of its important variables, but one must be able to evaluate the readiness with which all of the transport processes above take place.

b. Previous Work on Electrode Performance Studies

Thus far, several investigations have been performed in an attempt to determine the nature of the rate-limiting steps in fuel-cell electrodes.

Austin[1] made a very interesting analysis of concentration polarization effects within a diffusion electrode. His approach consisted of considering the idealized porous electrode geometry shown in Fig. 1, and postulating that the current density at any point of the electrode surface in contact with the electrolyte is a unique function of the electrode overpotential and the reactant's and reaction product's concentration at that point. Furthermore, Austin postulated that the electrode kinetics can be described by an expression of the form of the Tafel equation:

$$E - E_r = \eta = a + b \log i. \qquad (1)$$

Here, the reversible electrode potential E_r is obtained from the Nernst equation for the

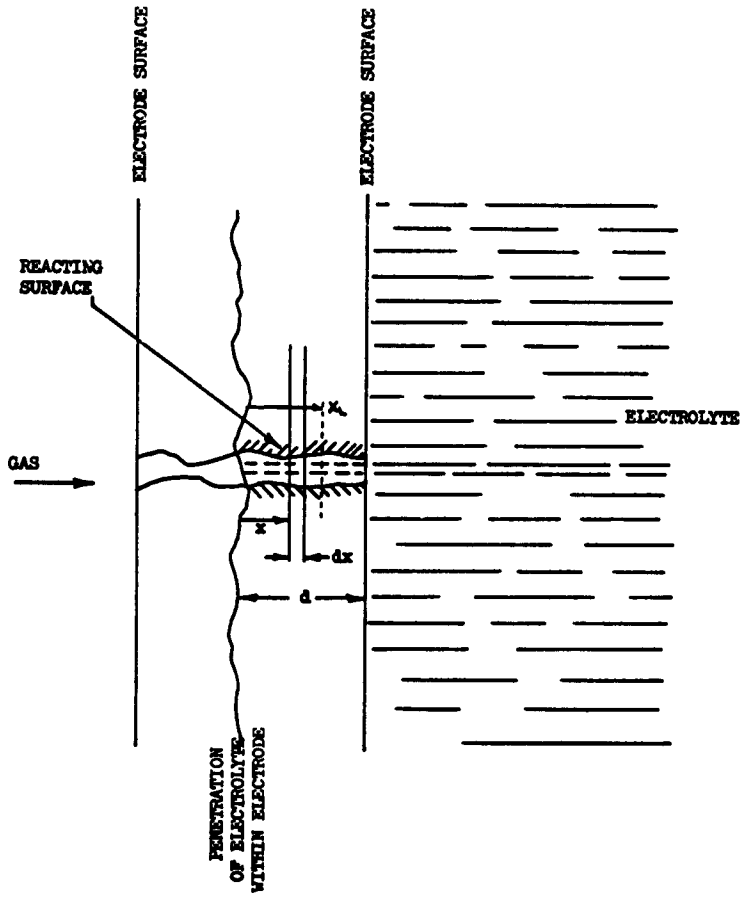

Fig. 1. Illustration of porous system.

reaction under consideration. Unfortunately, Austin's analysis is not applicable to the present oxygen-electrode performance studies because, as will be shown, over the range of interest the oxygen electroreduction does not follow a voltage-current relationship characterized by the normal Tafel equation. Furthermore, Austin's analysis considers the case in which the diffusion of reactants from the bulk of the electrolyte to the electrode-electrolyte interface is limiting, while in the present case we are concerned with the diffusion of the reacting gas to the electrode-electrolyte interface as the main diffusion limitation.

Sama[2] studied the problem of low-temperature, low-pressure, liquid-electrolyte oxygen electrodes. Using partially submerged, air-depolarized electrodes in caustic cells, Sama found that the current obtainable was limited by the mass transport rate of oxygen through the electrolyte. By performing oxidation studies with a wiped, rotating, partially submerged oxygen electrode that was designed to eliminate the electrolyte's resistance to oxygen mass transport, he found that the oxidation rate of copper electrodes was sufficient to support an equivalent current density of 26 ma/cm^2. Sama's results are not, however, directly applicable to quantitative electrode-performance calculations, since a gas-diffusion electrode is not being alternately oxidized and reduced, but the "sorption" and electroreduction of oxygen take place simultaneously.

Gorin and Recht[3,4] studied the nature of the electrode process in a porous-electrode, molten alkali carbonate electrolyte fuel cell. By putting approximate numbers into a simplified geometrical model of their fuel-cell system, they analyzed the three possible mechanisms by which the reactant gases could reach the electrode-electrolyte interface, where the electrochemical reaction must take place:

(i) Diffusion of the gaseous reactants through a thin electrolyte film in the neighborhood of the gas-electrolyte interface.

(ii) Permeation of gas through the bulk electrode metal.

(iii) Surface diffusion along the electrode surface.

The conclusion reached by Gorin and Recht was that mechanism (ii) is the most important one, and their calculations compared favorably with the operating data obtained from the actual fuel-cell systems. No specific experiments confirming the transport mechanisms postulated are reported. It is opportune to point out that the permeability of metals to gases decreases by several orders of magnitude as the temperature is lowered from 600-750°C to 25-100°C, since the diffusion of gases through metals is an activated process, with activation energies of the order of 10,000-40,000 cal/gram mole, that depends on the gas-metal system considered. This means that the above-postulated mechanism (diffusion of reactant gases through the bulk electrode metal) can in no way explain why appreciable current densities (100 ma/cm^2, or more) are possible in low-temperature fuel-cell systems.

Working under Justi, Grunberg[5] and Winsel[6] studied the nature of the electrode process in the D.S.K. low-temperature, porous-electrode fuel cells. They considered that the reaction takes place at the "active three-phase zone," and postulated (for the H_2-O_2

system) a mechanism by which chemisorbed gas diffuses along the pore walls to this three-phase reaction zone. No significant experiments are mentioned that confirm this mechanism, and no quantitative current-density calculations were made.

Yeager[7] studied experimentally the performance of graphite oxygen electrodes on aqueous electrolytes. Particular emphasis was placed on the study of reaction mechanisms, oxygen transport problems, and lyophobic properties of the electrodes. Yeager correlated actual electrode performance with some physical properties, such as electrode pore-size distribution, electrolyte flooding, and so forth, but did not attempt a quantitative analysis of the postulated electrode models.

c. Oxygen-Electrode Kinetics

The cathodic reduction of O_2 is one of the few electroreductions that has received detailed attention. Let us look at the over-all oxygen-electrode reaction:

$$O_2 + 2H_2O + 4e^- \rightleftharpoons 4\ OH^- \qquad \text{in base}$$

$$O_2 + 4H_3O + 4e^- \rightleftharpoons 6H_2O \qquad \text{in acid}$$

as compared with the hydrogen-electrode reaction:

$$2H_3O^+ + 2e^- \rightleftharpoons H_2 + 2H_2O \qquad \text{in acid}$$

$$2H_2O + 2e^- \rightleftharpoons H_2 + 2\ OH^- \qquad \text{in base.}$$

The fact that the oxygen-electrode reaction involved the transfer of four electrons would lead us to expect that the mechanism of this reaction should be more complicated than that of the hydrogen electrode. Furthermore, consideration of other products which could be formed throughout the reaction to complicate the formal reaction equilibrium corroborates this expectation. We must keep in mind that the reaction steps on which an electron transfer is involved do not occur freely in the homogeneous solution, so that the metallic phase will have to act as a catalyst. This involves some intimate kind of association between the species involved and the electrode, and the properties of the metal phase must be taken into consideration.

By all means, not an exhaustive list[8] of entities that might participate in the reaction in an aqueous electrode is:

$$O,\quad OH,\quad H_2O_2,\quad HO_2^-,\quad HO_2,\quad O_2^-$$

either in "free" or adsorbed states, as well as surface oxides, peroxides, and so forth. This system, therefore, can hardly be considered a simple one. The oxygen-electrode mechanism has been the subject of a great amount of study and controversy for some time. An understanding of its behavior has been sought for its application in analytical

chemistry, in the determination of dissolved oxygen concentration in solution by polarography. The recent interest in fuel cells has reawakened interest in the oxygen-electrode behavior, and significant developments concerning this matter are going on.

Thermodynamic Considerations

The half-cell reaction for oxygen electroreduction can be expressed as

$$O_2 + 4H^+ + 4e^- \rightleftharpoons 2H_2O_{(l)}.$$

The expression for the half-cell voltage by the use of the Nernst equation is

$$E = E^o - \frac{RT}{4F} \ln \frac{(aH_2O)^2}{(aH^+)^4(aO_2)}.$$

The standard oxygen electrode is thus one in which oxygen at unit fugacity is in equilibrium with water at unit activity, and hydrogen ions at unit activity. In this case the electrode potential is identical with the standard emf of the hydrogen-oxygen cell, which can be evaluated thermodynamically.

$$\tfrac{1}{2}H_{2\,(\text{ideal, 1 atm})} + \tfrac{1}{4}O_{2\,(\text{ideal, 1 atm})} = \tfrac{1}{2}H_2O_{(\text{liq})}$$

for which ΔF^o at 25°C is -28.345 K Cal, and

$$E^o_{cell} = \frac{-\Delta F^o}{nF} = \frac{28.345 \times 4.1840}{96.493} = 1.229 \text{ volt} = E^o_{O_2,H^+}.$$

If the activity of the water does not depart from unity, and if gaseous nonideality is ignored, the oxygen electrode potential will be given by

$$E_{O_2,H^+} = E^o_{O_2,H^+} + \frac{RT}{4F} \ln pO_2 + \frac{RT}{F} \ln aH^+.$$

If the partial pressure of oxygen, pO_2, with which the electrode is in equilibrium, has the standard value of 1 atm, then at 25°C

$$E_{O_2,H^+} = 1.229 - 0.05916 \text{ pH}$$

as measured against a standard hydrogen electrode (S.H.E.), in which the arbitrary zero of electrode potential at any temperature is defined as the potential corresponding to the reversible equilibrium between hydrogen gas at one standard atmosphere and hydrogen ions at unit activity.

Review of Published Work

Many attempts have been made to set up a reversible oxygen electrode. Until quite recently, all of these attempts have invariably been unsuccessful in room-temperature and aqueous-electrolyte systems.

In general, the different experimenters found that in measurements of the electromotive force of the oxygen half-cell, using any arbitrary reproducible half-cell as a reference electrode (H_2, calomel, Hg-HgO, etc.), in which oxygen was contacted with an unattackable electrode in the vicinity of room temperature, the value calculated for the reversible oxygen half-cell could not be obtained. The value obtained was approximately 1.0 volt for the oxygen-hydrogen couple, as compared with the thermodynamic value of 1.23 volts. Moreover, these values were not constant and reproducible, but drifted with time, and were very sensitive to the past history of the electrode (pronounced hysteresis effects with both O_2 pressure and current changes).

Haber,[9,10] using platinum electrodes separated from one another by an "electrolyte" consisting of glass or porcelain, between 300°C and 1000°C, and supplying steam plus H_2 and steam plus O_2 mixtures to each electrode, obtained values in close agreement with those calculated for a reversible cell. This is not surprising because at such high temperatures we would expect ready establishment of equilibrium conditions at the electrodes. For oxygen gas at low temperature, however, the electrode process is so slow that great experimental difficulties exist in the measurement of a true "equilibrium" or open-circuit reversible potential. Until quite recently, several theories have been widely accepted to explain the "inherent irreversibility" of the oxygen-electrode reaction. One of these theories held that the unattackable electrode is not completely inert toward oxygen, but is covered with an oxide film and never becomes completely saturated with oxygen. It was found by Grube[11] that PtO and PtO_2 electrodes gave potentials of 0.99 volt and 1.011 volts, respectively, which makes the situation similar to that for a platinum electrode surrounded by oxygen gas. Hoar,[12] on the other hand, maintained that the low value of the potential is due not so much to the presence of an oxide film as to its permeability, which gives rise to an internal current between the metal and the oxide film. According to this theory, adsorbed oxygen on the oxide film will render the surface cathodic toward the metal that is not in contact with oxygen. A current will flow between film and metal, together with cathodic solution of oxygen at the film surface, with consequent drop in potential. Hoar measured the cell potential while applying cathodic and anodic polarizing currents to his electrode, and obtained the corresponding Tafel lines. Extrapolation of these Tafel lines yielded an equilibrium value of 1.20 volts at a current density of $\sim 10^{-13}$ amp/cm^2.

The recognition of the fact that the oxygen-electrode reaction proceeds with great difficulty at room temperature as compared with a variety of other electrochemical reactions led Bockris and Huq[13] to the realization that any impurities present in such a system might be able to support electrochemical reactions of their own, and thus

yield misleading information on the behavior of the electrochemical reduction of oxygen itself:

> "The unattainability of the reversible O_2 electrode in normally purified solution is due to the fact that the velocity of simultaneous electrode reactions between impurities in these solutions and the electrodes is much greater than the exchange current for the oxygen evolution reaction ..."

Operating with solutions that had been painstakingly purified to the point at which they contained less than 10^{-11} mole/liter of impurities, Bockris and Huq were able to observe the reversible oxygen-electrode potential, and to determine the true exchange-current density for the reaction to be of the order of $1\text{-}3 \times 10^{-10}$ amp/cm^2, the value depending on the nature of the solution (0.1-0.001 N H_2SO_4).

In 1943, Berl[14] observed that on activated carbon electrodes, which do not catalyze the decomposition of hydrogen peroxide, the product of the electrochemical reduction of oxygen was hydrogen peroxide, and was led to postulate the following steps for the electrode reaction:

$$O_2 + H_2O + 2e^- \rightleftharpoons HO_2^- + OH^-.$$

It should be pointed out that the Berl reaction proceeds with great facility as compared with the oxygen-electrode reaction proper. Why, then, is the exchange current of the Berl reaction very high, whereas that of the oxygen electrode proper is vanishingly small?

One explanation may be that probably the latter involves the breaking of the interatomic bond in molecular oxygen:

$$O_2(g) \rightleftharpoons 2O(g), \quad \Delta G^\circ = 110 \text{ K Cal.}$$

This breakage does not occur in the Berl reaction. This has been shown to be true by the use of isotopically discriminated oxygen.[15] In both anodic and cathodic processes, the O-O is exchanged between molecular oxygen and hydrogen peroxide with bond modification, but not breakage, and there is no exchange with the oxygen of H_2O or OH^-. This places a limitation on the possible mechanisms that take place in the Berl reaction, since all reaction steps involving the O-O bond breakage should be ruled out.

Weisz and Jaffe[16] confirmed the fact that oxygen is electrochemically reduced to hydrogen peroxide, and not to water, in alkaline solutions, and that the hydrogen peroxide formed decomposes catalytically into water and oxygen. They also ascertained the fact that in both acid and basic solutions, when hydrogen peroxide and oxygen both compete for electrons, the rate of reduction of the latter is much greater than that of the former.

Sawyer and Interrante[17] studied the electrolytic reduction of dissolved oxygen on different metal electrodes and in several electrolyte systems. From the results of both voltammetric and chronopotentiometric studies they concluded that the oxygen reduction at preoxidized electrodes is pH-dependent, and that for Pt, Pd, and Ni electrodes the

electrode reaction for oxygen reduction is

$$M(OH)_2 + 2e^- \rightleftharpoons M + 2\ OH^-.$$

The oxygen in solution then reoxidizes the electrode, which is then re-reduced. These conclusions agree with the work done by Lingane[18] on oxygen electroreduction at platinum electrodes, from which he also established the fact that platinum electrodes have a coating of $Pt(OH)_2$ or PtO_2.

Bianchi and others[19] studied the electroreduction of oxygen and hydrogen peroxide on different metal electrodes, and also arrived at the conclusion that surface oxides are formed in the presence of oxygen or hydrogen peroxide. They also found that both oxygen and hydrogen peroxide are reduced with much greater difficulty in acid solutions, and postulated that increased difficulty in the adsorption of oxygen or decomposition of hydrogen peroxide on the electrode surface is responsible for this phenomenon.

d. Hydrogen-Electrode Kinetics

The hydrogen electrode has been the subject of multiple studies. Since it is used as a standard reference electrode, a considerable amount of research has been performed to study its reproducibility and current-carrying characteristics. Early research on the corrosive oxidation of metals led to studies of the hydrogen-evolution reaction, and the hydrogen-electrode reaction has been chosen as the main source of experimental and theoretical research in electrode kinetics.

Tafel[20] was one of the first investigators to study the electrode kinetics of hydrogen evolution, and observed that over a wide region of current densities, the electrode overvoltage is a direct function of the logarithm of the current density. Detailed studies of the hydrogen-evolution reaction mechanism have been performed by Bockris and Conway,[21] Schuldinger and Hoare,[22,23] and Oikawa.[24] These studies are of no direct interest in the present problem, since we are concerned with the kinetics of hydrogen oxidation at current densities of the order of 10^{-4}-10^{-1} amp/cm^2, and the above-mentioned studies help only in the selection of a suitable electrode material, and in the general understanding of the problem.

Bockris and Conway showed that the exchange-current density for the hydrogen-electrode reaction of Pt, Pd, and Rh electrodes is extremely high (10^{-3}-10^{-4} amp/cm^2), and this indicates that the electrochemical kinetics are not likely to limit the electrode performance.

Cosjin[25,26] studied the problems associated with diffusion polarization of the hydrogen electrode, and considered the limitations imposed on the electrochemical reaction by both the diffusion rates of molecular hydrogen and the reacting ions. This work shows that either strongly basic or acid solutions that are necessary to permit the hydrogen electro-oxidation reaction are not limiting, and only concentration polarization or the hydrogen adsorption rate might impose limitations on the electrode operation.

1.2 ANALYTICAL AND EXPERIMENTAL APPROACH TO THE PROBLEM

In order to calculate the performance obtainable from a particular electrode system, one must be able to predict both the mass-transport phenomena and the kinetics of the electrode reaction itself. For an idealized (but representative) electrode geometry, there are no major difficulties involved in calculating the mass transfer. The electrode kinetics, however, are not available from the work thus far reported, since most of the studies reviewed here involved oxygen-electroreduction studies at current densities far too low to be in our range of interest, which is 10^{-4} amp/cm^2, and higher. The few investigators who performed experiments at current densities above 10^{-4} amp/cm^2 did not work with controlled and known mass-transfer conditions, and thus were not able to suitably separate the mass-transfer from the kinetic effects.

For the present work, an experimental apparatus was devised that permitted the study of the electrochemical kinetics under known mass-transfer conditions. In this system the partial pressure (or equivalent concentration) of the reactants and reaction products at the electrode surface can always be estimated. After obtaining the required electrochemical kinetic data, it was possible to undertake the desired performance calculations for some electrode systems of idealized geometry.

II. PROCEDURE

2.1 EXPERIMENTAL APPARATUS

a. Steady-State Voltage vs Current-Density Measurements

In order to investigate separately the electrochemical kinetics and the mass-transfer effects in an electrode system, the apparatus shown in Fig. 2 was constructed. This apparatus consists of a pressure saturator, where liquid electrolyte is saturated with a reactant gas at any desired reactant partial pressure at room temperature, by bubbling the gas through a fritted glass plug located at the bottom of the saturator. The pressure in this vessel is controlled through a pressure regulator located upstream. During a run, the electrolyte is throttled through the valve V_1, metered by the flowmeter F through the test electrode T, and exhausted out the cell overflow O. This system therefore makes possible the flow of electrolyte saturated with a gas at a desired partial pressure through the electrode at a controlled and known velocity, permitting the calculation of the mass transfer from the liquid to the electrode surface.

During a run, a current is passed through the test electrode T by means of the dc power supply B, decade resistance R (from 1 ohm to 106 ohms), and the dummy electrode D. The current flowing through the test electrode is measured by means of the ammeter A. The advantage of using a dummy electrode and auxiliary power supply instead of another fuel-cell electrode is that in this way the current density can be controlled at will, and can be made independent of the test-electrode performance by having a large enough dc power source. As far as the test electrode is concerned, the presence of the dummy electrode instead of any other fuel-cell electrode does not make any difference because the test electrode reaction is exactly the same, as long as no reaction products from the dummy electrode (if they were to depolarize the test electrode) are allowed to reach the electrode that is under study. The electrode potential at any given current density is measured against a calomel reference electrode by means of a Luggin capillary connected through a salt bridge to this reference electrode. The potential difference between the test and the reference electrodes is measured either with a Sargent Model MR DC Recorder, or a Tektronix Model 502 dual-beam oscilloscope.

b. Double-Layer Capacitance Measurements

In order to clarify the mechanism of some electrochemical reactions, it is useful to measure the electrical double-layer capacitance at the electrode surface under the operating conditions of interest. Changes in the electrical double-layer capacitance often reflect changes in its structure, such as the formation, elimination or replacement of adsorbed species at the electrode surface, the formation of surface oxides, and so forth.

In this study a system like the one used by Hackermann[27,28] was employed, and the circuitry involved is outlined in Fig. 3. The test cell is exactly the same as the

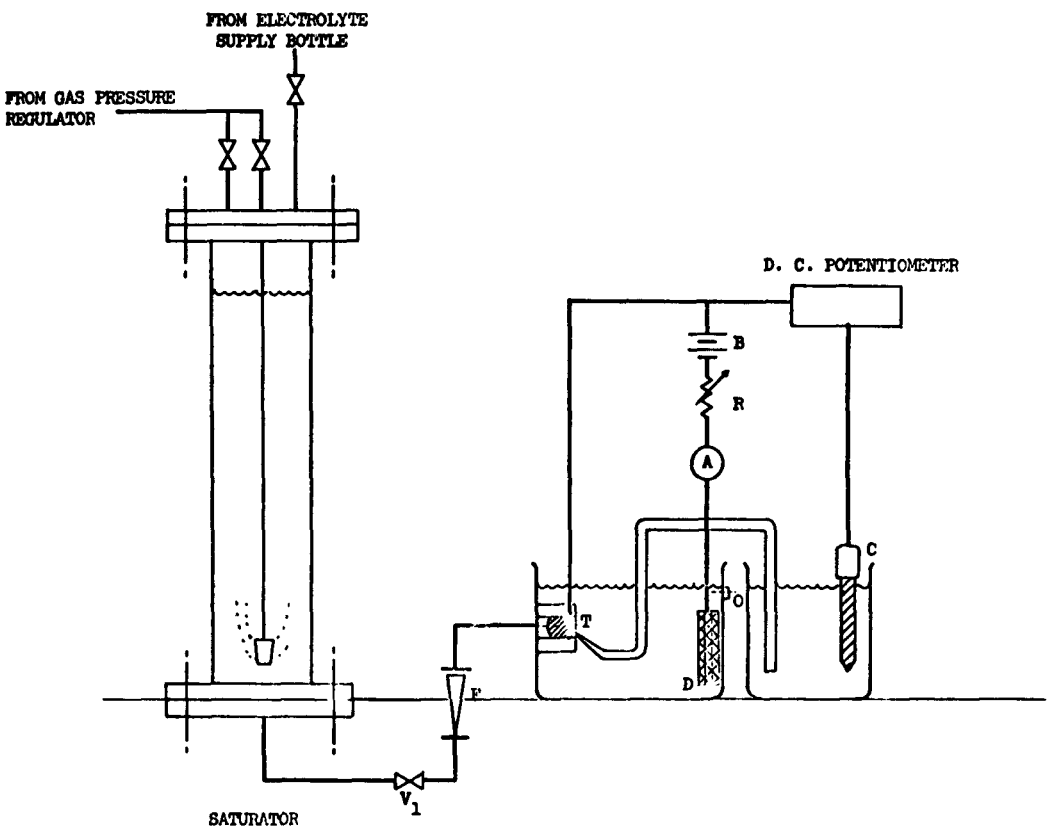

Fig. 2. Schematic diagram of experimental apparatus.

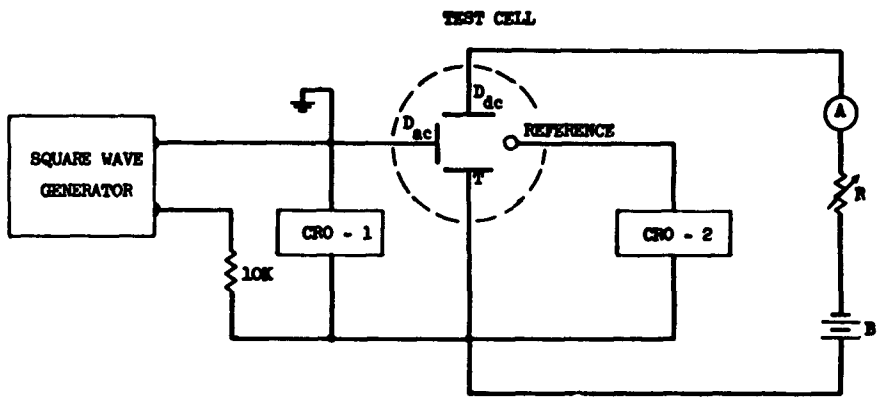

Fig. 3. Circuit for the double-layer capacitance measurements.

one shown in Fig. 2, and similarly any desired dc current load can be imposed on the system by means of the dc power source B, decade resistance box R, and the dummy electrode D_{dc}. The electrode potential is monitored against a calomel reference electrode, and this potential is displayed by one of the two beams of the dual-beam cathode-ray oscilloscope. Simultaneously, a 1000-cps square-wave signal is superimposed on the direct current through T, by means of a Hewlett-Packard Model 202A low-frequency signal generator, and dummy electrode D_{ac}. This signal is small enough in amplitude (1.5 mv) so that it does not interfere with the electrode process itself. It was shown by Frumkin[29] that ac signals of up to 15-mv amplitude can be used in these measurements without seriously affecting the double-layer capacitance values.

The electrode system can be approximated by

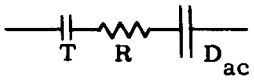

The output of this signal after it goes through this electrode system is displayed by means of the second oscilloscope beam, and shows the slope of the double-layer charging and discharging curves. At any desired operating condition, the cathode-ray oscilloscope picture is photographed by means of a Polaroid camera attachment, which yields a permanent record of both the charging curves and the electrode potential vs the calomel reference electrode. A sample calculation from one of these pictures is presented in Appendix B.

2.2 EXPERIMENTAL PROCEDURE

a. Comparative Experiments between Flooded and Nonflooded Electrodes

Electrode-potential vs current-density curves were obtained for the electroreduction of oxygen in a Kordesh type of electrode in 20% KOH. These curves were obtained by operating at a certain current density until a steady-state potential (achieved in a few seconds) was reached. Potentials were measured going both up and down in current density, to study their reproducibility.

These performance curves were obtained first with the Kordesh type of electrode horizontally immersed in the liquid electrolyte, with sufficient O_2 back pressure to preserve a stagnant gas-liquid interface somewhere within the electrode (no gas bubbling through). Similar curves were obtained for the same electrode with oxygen bubbling through the electrode at varying flow rates. Finally, the electrode performance was studied when electrolyte saturated with oxygen was made to flow through the porous electrode. The purpose of these tests was to investigate the extent to which the electrode performance will be dependent on operating conditions, such as oxygen flow rate, position of the gas-liquid interface, and so forth.

b. Experiments with Screens

All of the electrochemical kinetic studies were performed with electrodes that consisted of a stack of wire screens of the catalyst material that was studied, such as silver or platinum. The reason for employing metal-screen electrodes was that the total catalyst metal surface is known, and thus basic reaction-rate data can be obtained. Furthermore, the screen geometry is simple enough to permit reasonably accurate calculations of the mass-transfer coefficients from the bulk liquid to the electrode surface. Such pure metal screens are also excellent electrical conductors, and keep the whole electrode surface at a constant potential, thereby simplifying the interpretation of the results.

The variables studied were: reactant concentration, electrolyte flow rate and temperature, and electrode geometry. The specific experiments that were performed are described and discussed and the results are given in Section III.

III. RESULTS OF EXPERIMENTS

3.1 COMPARATIVE EXPERIMENTS WITH FLOODED AND NONFLOODED ELECTRODES

The results obtained from testing a 0.25-in. thick Kordesh type of porous carbon electrode (prepared as described in Appendix C) are shown in Fig. 4. These results were obtained by studying the oxygen electroreduction in 20% by weight KOH at 25°C. The electrode-potential vs current-density curves are shown for different operating conditions. Curve 1 represents the electrode performance when the oxygen-electrolyte interface is preserved stagnant, and thus is typical of the conditions under which gaseous-diffusion electrodes usually operate. As the oxygen flow rate is increased, and oxygen gas bubbles through the electrode, the oxygen-electrolyte interface within the electrode fluctuates in position. Curves 2 and 3 show the electrode performance under these conditions. Curve 4 shows the electrode performance when the electrolyte is presaturated with oxygen and forced through the pores, thereby making a large fraction of the electrode surface available for the electrochemical reaction.

The curves were obtained by going both up and down in current density, and waiting for a steady-state electrode potential to be reached (which took 100 seconds at most). These potentials were found to be reproducible as long as the flow conditions were kept constant. No electrode lifetime tests were attempted. When presaturated electrolyte was flowing through the electrode, the flow rate was such that only approximately 50% of the total dissolved oxygen that was passed was consumed at the highest current-density point. The calculations of this "stoichiometric" limiting current density are shown in Appendix A.

These results demonstrate that under normal operation only a fraction of the total electrode area is available to support the electrochemical reaction. The increased fluctuation of the gas-liquid interface position makes it possible for the oxygen to reach parts of the electrode which would not otherwise have been available, by shortening the oxygen gas-active area diffusion path through liquid. Similarly, causing the presaturated electrolyte to flow through the electrode pores increases the ease with which oxygen can reach the electrode-electrolyte interface, since the diffusion path is limited to the distance between the center of the large pores and the surface of the micropores radiating from their walls. No liquid flows at any appreciable rate through the small pores because of pressure-drop limitations.

The increased availability of electrode area explains the increased limiting current densities as one goes from a stagnant interface electrode to other modes of operation.

Let us consider the idealized model shown in Fig. 1, which shows a pore of diameter d, completely filled with electrolyte up to the point $x = 0$ in the chosen coordinate system. Oxygen gas has to dissolve into the electrolyte and diffuse to the electrode-electrolyte interface before reacting. If we consider a long, narrow pore in which only the axial diffusional resistance is important, and if we make the simplifying assumption

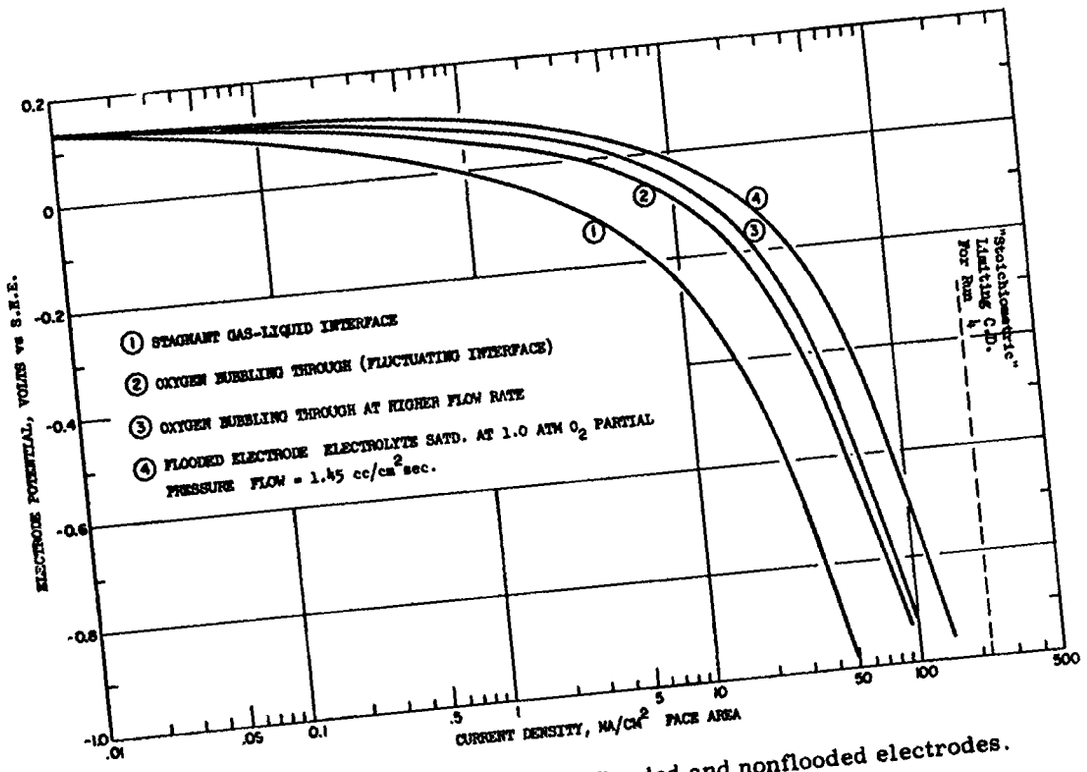

Fig. 4. Comparative experiments with flooded and nonflooded electrodes.

that the current density at the electrode surface is constant throughout the region that oxygen is able to reach by diffusion, it is possible to define an "effective pore length" x_L at which the electrochemical reaction stops for lack of oxygen. This analysis is analogous to the Thiele-Wheeler[30] approach for calculating the effectiveness of a porous catalyst, for a zero-order reaction. The total face area current density i_{tot} supported by a porous surface at a catalyst surface current density i_s will be limited by the oxygen mass-transport rate:

$$i_s \pi d(x_L - x) = \frac{dc}{dx} D_L \, 4F \, \frac{\pi d^2}{4}$$

$$i_{tot} = \frac{\pi d}{4d^2} (x_L - x)_{x=0} \, i_s$$

with the boundary conditions

$$\left.\begin{array}{l} c = 0 \\ \dfrac{dc}{dx} = 0 \end{array}\right\} \text{ at } x = \infty \qquad\qquad \left.\begin{array}{l} c = c_o \\ \dfrac{dc}{dx} = \dfrac{i_{tot}}{D_L \, 4F(\epsilon)} \end{array}\right\} \text{ at } x = 0.$$

Solving this differential equation between the limits $x = 0$ and $x = x_L$ and $c = 0$ and $c = c_o$, we find that the effective pore length x_L can be expressed as

$$x_L = \left(\frac{c_o D_L \, 2F(d)}{i_s} \right)^{1/2}.$$

This model also explains why the current-density differences at a given overvoltage are greatest at low over-all current densities for the different modes of electrode operation. At low current densities, most of the wetted micropore area is available to catalyze the electrochemical reaction, as long as oxygen-transport problems along the longer, larger pores are not serious. The mass transport through the larger pores is not limiting if bulk flow of saturated electrolyte through them, which is caused either by flow operation or gas bubbling through the electrode, exists. For a given voltage, the face area current density for the flow electrode is more than 10 times the current density for the stagnant interface electrode at low overvoltages (current densities). As the current densities increase, oxygen-transport problems along the smaller pores become appreciable (that is, the "effective length" becomes smaller than their actual length), and the effective increase in available electrode area is smaller.

It is clear, then, that the fraction of the electrode area which is being used effectively will vary with operating conditions, being sensitive to both the oxygen-flow conditions and current density. This complication makes it highly undesirable to use a conventional type of porous electrodes for studies in which actual current densities per unit surface area must be known.

3.2 ELECTROCHEMICAL KINETICS

a. Oxygen Electroreduction

Several experiments have been performed to study the oxygen electroreduction reaction on both silver and platinum wire screens, under conditions of varying flow, pH, temperature, and current density. The results are presented in electrode potential (versus the Standard Hydrogen Electrode, S.H.E.) vs current density graphs, the current density being plotted on a logarithmic scale, in order to show the electrode behavior over an adequately wide current-density range.

Typical Effects of O_2 Concentration and Electrolyte Flow Rate

Figures 5 and 6 show the effects of electrolyte-oxygen concentration and electrolyte flow velocity for platinum- and silver-screen electrodes, respectively. These runs were performed under such conditions that even at the highest current density no more than 10% of the oxygen in the flowing electrolyte was consumed, in order to have a constant oxygen-diffusion driving force throughout the electrode.

The results are quite similar for the two different metal electrodes. All of the voltage-log current-density curves shown here are characterized by an initial straight-line region at very low currents, followed by a region in which the overvoltages become greater at a progressively increasing rate, up to a point where the voltage-log current-density curve becomes nearly vertical. For each electrode we also find that the straight-line portion of these curves at low current densities is common to all runs, independently of oxygen concentration or electrolyte flow velocity; that is to say, the electrode potential is a function of current density only, and not of the oxygen supply conditions. The vertical portion of the curves, on the other hand, is strongly dependent on the oxygen concentration in the electrolyte and on the electrolyte flow velocity. Runs with electrolyte saturated at 1.0 atm with pure oxygen and with air (pO_2 = 0.21 atm) in which the electrolyte flows at the same space velocity through the screens for both cases, show that the location of this vertical region or drop-off in the curves differs by a factor of approximately 5 in the current-density scale, which would be expected if the oxygen mass-transfer rate from bulk electrolyte to the electrode surface were controlling. Runs at different electrolyte flow rates also show that the current density at this vertical region increases with a power dependence that is between the 0.6^{th} and the first power of the liquid flow rate.

Calculation of the oxygen mass-transfer rates to the electrode surface from values of oxygen solubility and diffusivity in potassium hydroxide that have been reported, and measured flow rates are listed in Appendix A. The results are presented in Table 1. These calculated limiting current densities check with the observed limiting current-density values, especially if we consider that the diffusivity and the solubility of O_2 in 20% KOH are not known very accurately, and if we take into account the approximations made in the mass-transfer calculations (approximating a screen system that flows

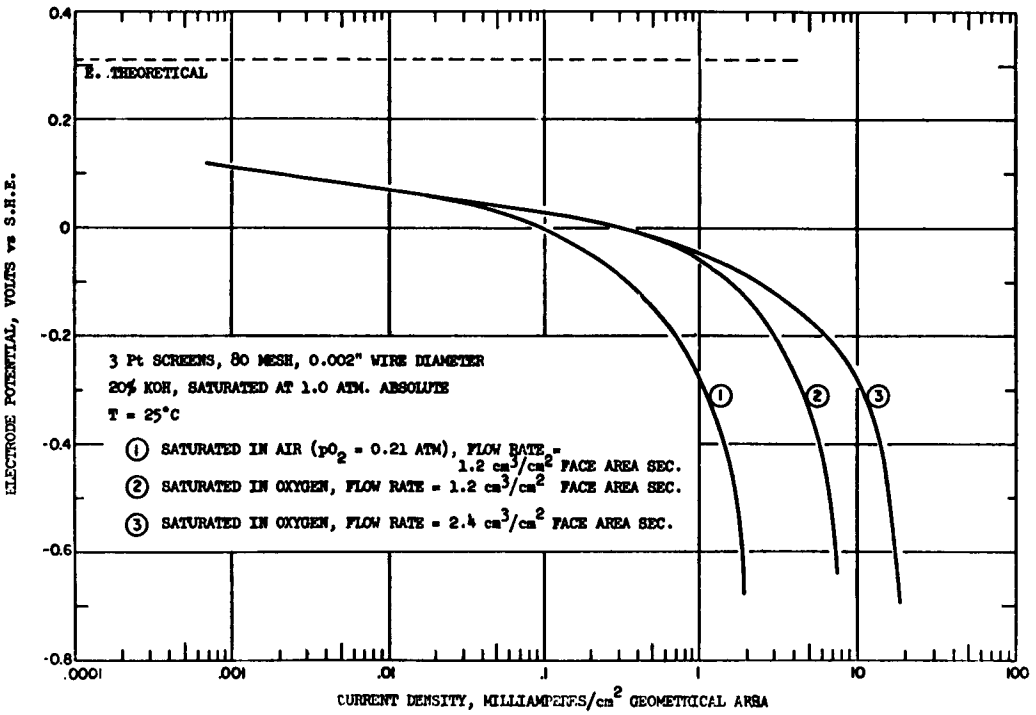

Fig. 5. Oxygen electroreduction on platinum screen, 20% KOH.

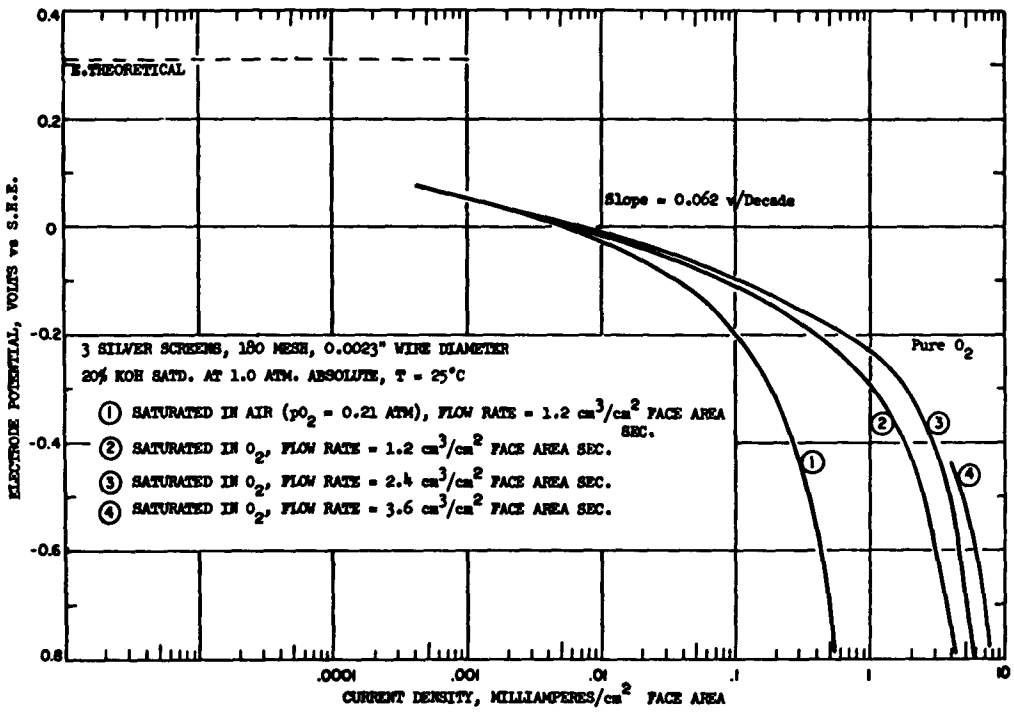

Fig. 6. Oxygen electroreduction on silver screen, 20% KOH.

Table 1. Results of Calculations of Mass-Transfer Rates and Measured Flow Rates.

Figure No.	Run No.	Calculated I_L	Observed I_L
5	2	2.0×10^{-3}	6×10^{-3}
5	1	4.2×10^{-4}	1.5×10^{-3}
6	2	3.5×10^{-3}	4×10^{-3}
6	1	7.4×10^{-4}	6×10^{-4}

normal to a cylinder of the screen wire diameter). The results of Table 1 confirm the explanation that the final electrode potential drop-off is caused by oxygen-concentration polarization.

The linear portion, at low current densities, of all of the presented electrode potential vs logarithm of the current-density plots has been measured for a wide enough current-density range to be clearly defined. Here the voltage-current density behavior of the oxygen electrode can be described by the conventional Tafel equation,

$$E_{rev} - E_{act} = \eta = a + b \log i \tag{2}$$

in which it is assumed in its derivation[20] that one single electrochemical reaction step is rate-controlling. In this region, therefore, the electrochemical kinetics controls the process, and the mass-transfer limitations are unimportant.

If the electrodes studies concerned systems in which the electrode reaction is completely governed by the electrochemical kinetics up to the point where concentration polarization becomes appreciable, the voltage versus log current-density plots would have the general shape shown in Fig. 7. Curves of this shape will be encountered, in Fig. 19, for peroxide systems.

The electrode potential would follow the Tafel equation as far as close to the point where concentration polarization sets in, and then it would drop off quite sharply. This is evident from the form of the Nernst equation which describes the effect of reactant concentration on the reversible electrode potential:

$$E_{rev} = E_o - \frac{R\,T}{n\,F} \ln K \tag{3a}$$

or

$$\Delta E_{rev} = \frac{R\,T}{n\,F} \ln \frac{c_o}{c_s} \tag{3b}$$

Until the reactant concentration at the electrode surface c_s becomes much smaller than the bulk reactant concentration c_o (that is, it approaches zero), the reversible electrode

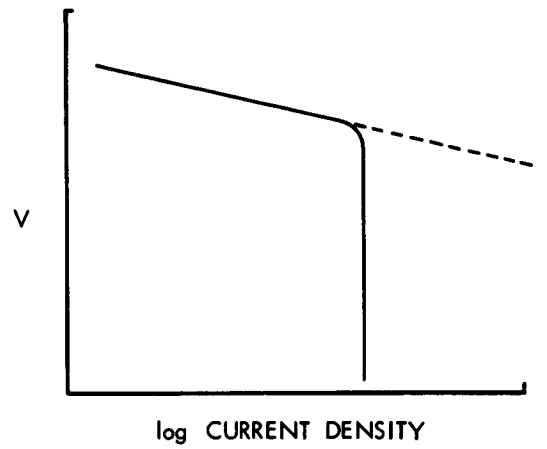

Fig. 7. Expected voltage vs log current-density curve.

potential will remain unchanged, and the actual electrode potential will follow the same Tafel line. As the current density increases, and the reactant concentration drop through the mass-transfer boundary layer increases, no appreciable concentration polarization occurs, up to the point at which nearly the total available concentration driving force (c_o-0) is required to diffuse enough oxygen to support the electrochemical reaction. At that point the oxygen concentration at the electrode surface rapidly drops to zero with a small increase in current density, and the reversible electrode potential changes very sharply. This change is very sharp because of the logarithmic form of the Nernst equation. As the reversible electrode potential changes, it can be seen from Eq. 2 that the actual electrode potential at a given current density must also change by the same amount.

As it can be seen in Figs. 5 and 6, the transition from a normal Tafel-equation behavior to oxygen-concentration polarization is not so sharp, and a gradually increasing deviation from the Tafel line sets in at approximately one-tenth of the limiting current density. This deviation is quite evident, and can be explained in terms of a mechanism that also explains why at low current densities (in the Tafel region) the oxygen-electrode potential seems to be insensitive to the oxygen partial pressure, contrary to what the Nernst equation would suggest. This deviation is not attributable to the existence of a mixed electrode potential because no other reaction besides the oxygen electroreduction reaction can take place until the hydrogen evolution potential is reached in the solution that is being studied.

The oxygen-electroreduction studies performed by Lingane[18] and by Sawyer and Interrante[17] suggested that before the electroreduction step oxygen reacts with the metal electrode to form either a surface oxide or hydroxide like PtO, PtO_2 or $Pt(OH)_2$ in Pt electrodes. The available evidence does not justify attributing such a definite identity to this metal-oxygen intermediate. It is more appropriate to postulate the existence of

"chemisorbed" oxygen on the metal-electrode surface, and that this chemisorbed oxygen at the electrode surface is the species that is electrochemically reduced. We are thus postulating a chemisorption step to be necessary before the electrochemical reaction step:

(a) $O_2 + {}_xM \longrightarrow {}_xM \ldots O_2$ Adsorption

(b) $2H_2O + {}_xM \ldots O_2 + 4e^- \longrightarrow 4\ OH^- + {}_xM$ Electroreduction

For this model two effects would yield the gradually increasing deviations from the Tafel line observed before concentration polarization is reached.

Assume that the oxygen chemisorption rate on the electrode surface can be described by the Becker-Zeldovich equation,[31,32] which has been found to apply to the chemisorption of oxygen on silver[32] and the desorption of oxygen from tungsten[33]:

$$\text{Adsorption rate} = \frac{d\theta}{dt} = a(c_s)(1-\theta)\, e^{-b\theta}, \tag{4}$$

where θ is the fractional coverage of the surface active sites by the chemisorbed oxygen, and t is time. In steady state, the rate of oxygen chemisorption is equal to the rate of adsorbed oxygen electroreduction (under the assumption that the chemisorption is essentially irreversible, that is, the desorption rate is negligible).

$$\frac{iB}{nF} = \frac{d\theta}{dt} = a(c_s)(1-\theta)\, e^{-b\theta} \tag{5}$$

Therefore, a given electrode current density i and oxygen concentration at the electrode surface c_s characterize a surface coverage θ. If we recall from our postulated mechanism that the electrochemical reaction can take place at the areas covered by chemisorbed oxygen, it will be more appropriate to use an "effective" current density based on "effective" or covered area, instead of the current density based on total electrode area, whenever considering the electrochemical kinetics. The "effective" current density can be described by the relation

$$i_{eff} = \frac{i_s}{\theta}. \tag{6}$$

At a given bulk electrolyte-oxygen concentration, as the current density increases, the oxygen chemisorption rate is not fast enough to keep the electrode surface completely covered, and the coverage θ becomes smaller than unity. The "effective" current density is thus larger than the current density based on total surface area, with the consequent increase in the electrode overvoltage.

The low chemisorbed oxygen coverage at current densities close to the limiting current density has an additional effect on the electrode overvoltage, since the activation energy of adsorption is not independent of the coverage θ. Higuchi, Eyring, and Ree[34] showed that the activation heats of adsorption and desorption generally decrease with increasing θ, and explained this fact as being due to the effect of the field of the adsorbed

layer on the adsorbing (desorbing) atom or molecule. Other investigators explain this phenomenon by postulating that some sites on the surface have higher activity than others. Whatever the real explanation in this case is, it would be expected that as the coverage decreases only the more strongly bonded chemisorbed oxygen would be left, and hence a higher than normal activation energy (overvoltage) would be required for the electroreduction step. We thus find two effects: (a) increased effective current densities, and (b) increased activation energies, which explain the abnormally high overvoltages as the limiting current densities are approached, if we accept the explanation that over this region the oxygen sorption rate becomes controlling.

The proposed explanations of the electrode behavior are quite consistent with all of the experimental evidence. It is desirable, however, to find some more supporting experimental evidence for the proposed explanation. Unfortunately, it is not easy to ascertain the presence and amount of chemisorbed species on an electrode surface in the presence of electrolyte, under varying current densities and oxygen concentration at the electrode surface. Studies of the electrode surface by infrared spectroscopy are not possible with present methods, since the large amounts of electrolyte in the beam path would drown out the signal obtained from a chemisorbed monolayer. The only method that yields some information on the state of the electrode surface is an indirect one – electrode double-layer capacitance measurements. The presence of a layer of chemisorbed oxygen on the electrode surface should affect the electrode double-layer capacitance. Thus, if we postulate that the coverage, θ, of chemisorbed oxygen changes throughout the current-density range on which deviations from the Tafel equation are observed, it would be expected that the electrical double-layer capacitance should change as well. These electrical double-layer capacitance measurements have been performed, by the methods described in section 2.2b. The results are presented in Fig. 8, in which the electrical double-layer capacitance has been measured as a function of current density, at a constant electrolyte velocity, with electrolyte saturated in oxygen at 1 atmosphere in one case, and in air (pO_2 = 0.21 atm) in the other. These results show that indeed the electrical double-layer capacitance begins to change noticeably at the same point at which the voltage vs current-density curves for that particular experiment begin to deviate from the normal Tafel line. We find that the electrode double-layer capacitance (coverage) is not a function of current density alone, but of both current density and oxygen concentration at the electrode surface, as would be expected from Eqs. 2, 5, and 6, an observation that tends to confirm the proposed explanation.

The fact that the electrode potential at low current densities appears to be independent of oxygen concentration (partial pressure) can now be explained. From the Nernst equation we would expect the oxygen electrode potential at equilibrium to differ by

$$E = \frac{RT}{nF} \ln \frac{1.0}{0.21} = 0.0104 \text{ volt}$$

between electrolyte saturated with oxygen and air. Differences of such magnitude are

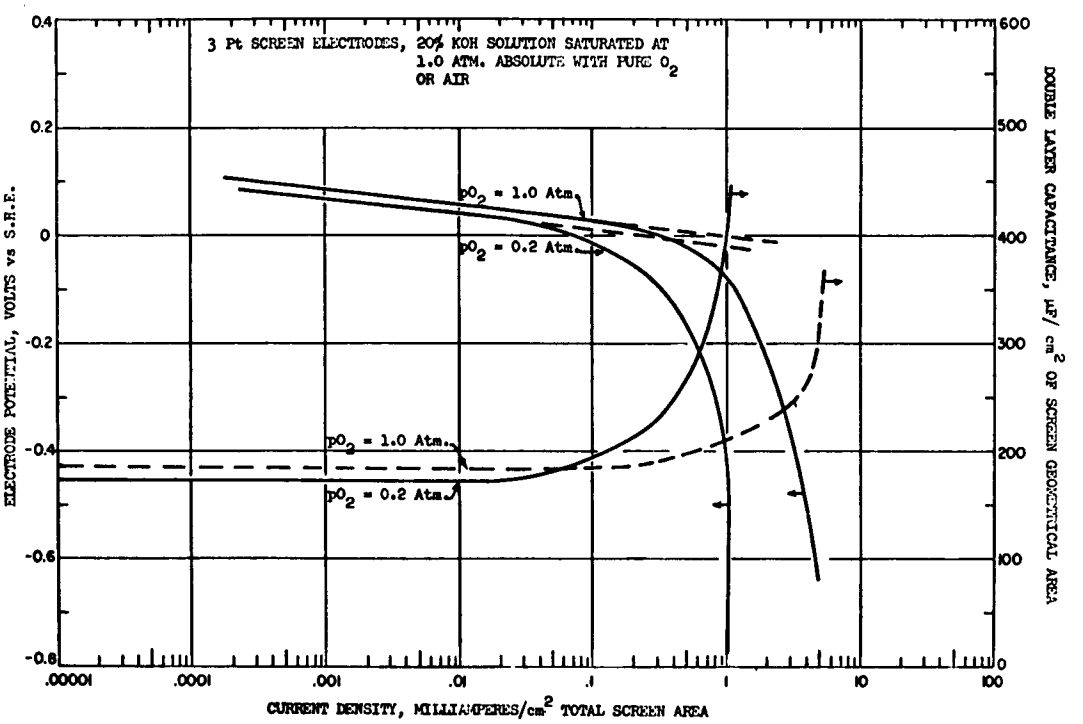

Fig. 8. Double-layer capacitance measurements on a platinum oxygen electrode.

not observed in Figs. 5, 6, and 8 in spite of the fact that the recorder sensitivity is approximately 0.002 volt. This can be explained on the basis that at low current densities, the electrode surface is saturated ($\theta = 1.0$) at both oxygen partial pressures, and the activation energy required to reduce the chemisorbed oxygen from the electrode is the same for both cases, making the electrode overpotential the same.

Runs with Different Numbers of Screens

Runs were performed with different numbers of screens stacked together to form an electrode, in order to show that the current density per unit total area, and not the current density per unit face area, determines the electrode potential. The purpose of these runs was also to find out to what extent the stacking of screens together affected the flow conditions, and thus affected the mass-transfer coefficients. The stacking of screens could have the additional effect of blocking off some electrode area, and we considered it desirable to show whether or not this effect would be appreciable.

Calculations in Appendix A show that even with 27 screens at the highest current density measured only 52% of the total available oxygen supplied in the electrolyte was consumed, and it can be said that in these experiments the oxygen concentration in the electrolyte was held essentially constant throughout the electrodes.

The results of runs with 1, 3, 9, and 27 screens are summarized in Figs. 9 and 10. At a given overvoltage, the current density per unit electrode face area is directly proportional to the number of screens. The current density per unit screen total area is constant, regardless of the number of screens used.

From these results it can be concluded that if there is any appreciable change in the liquid-screens mass-transfer coefficient when stacking several screens together, this effect is offset by the blocking off of some electrode area as the screens are stacked in contact with each other.

If the number of screens were to be increased greatly by more than 30, ohmic drops through the electrolyte inside the thick electrode structure would become appreciable.

Effect of Temperature on Electrode Performance

Two runs were performed on three stacked silver-screen electrodes, with 20% by weight KOH solution saturated with oxygen at 1.0 atm absolute pressure, 25°C, and flowing at an identical mass flow velocity. In one run the electrolyte temperature past the electrode was 25°C, and in the other the electrolyte was heated to 57°C by the time it flowed past the electrode. The results of these runs are presented in Fig. 11.

As would be expected, increased temperature has the effects of causing a rise in the limiting current density (increase in diffusivity, decrease in solution viscosity) and in lowering the overvoltage at low current densities, since the electrochemical reaction is an activated process. The second effect, however, is hard to ascertain quantitatively, since it implies a decrease in the slope of the Tafel line by a factor of only $e^{298/330} = 0.74$, and such a slope is not

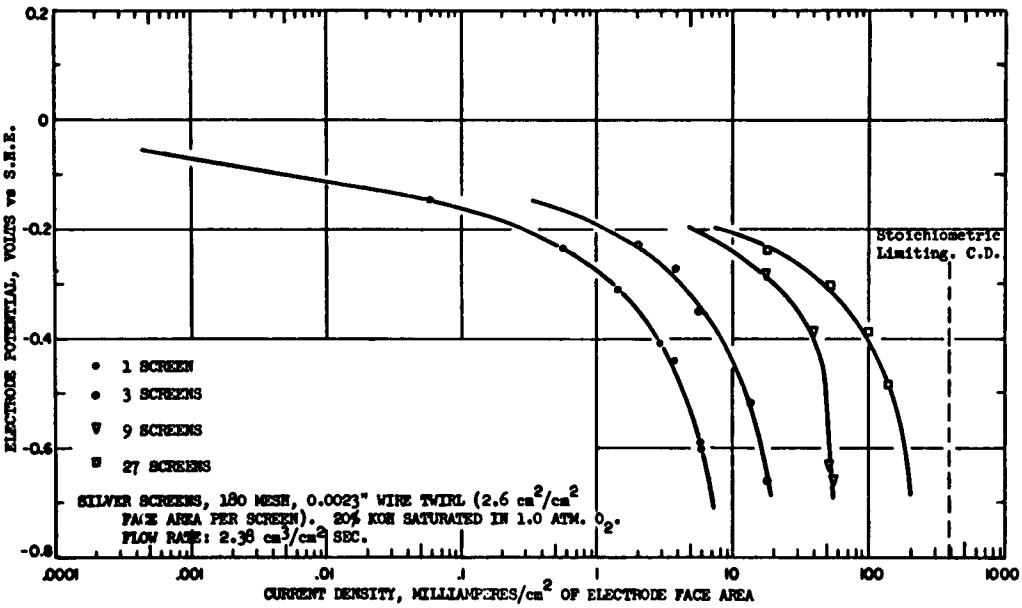

Fig. 9. Experiments with multiple screens.

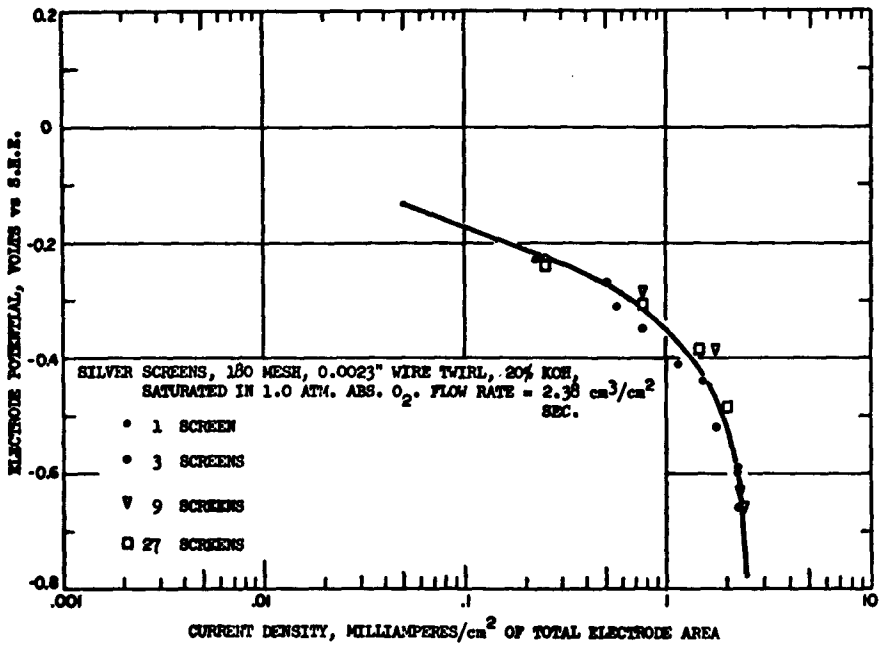

Fig. 10. Experiments with multiple screens.

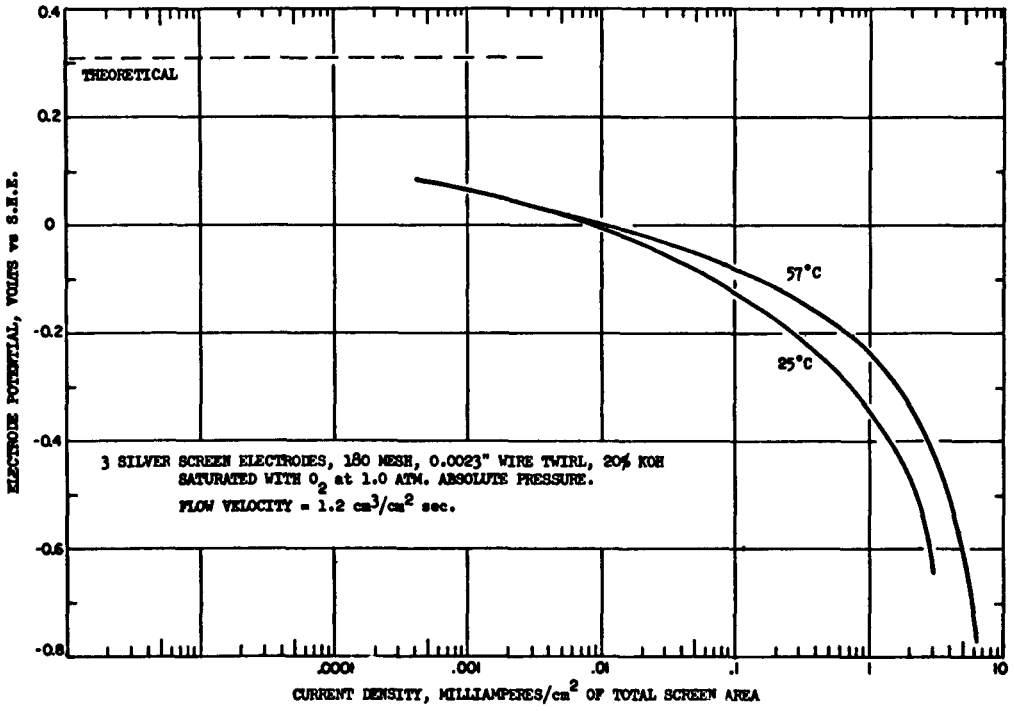

Fig. 11. Effect of temperature on electrode performance.

known with sufficient accuracy in both runs to permit a quantitative evaluation.

As far as the location of the limiting current density is concerned, we have a $(330/298)^{3/2} = 1.17$ factor increase in the diffusivity of oxygen in KOH, plus a fivefold decrease in the electrolyte viscosity. The increase in the mass-transfer coefficient thus should be

$$\frac{k_{new}}{k_{old}} = (1.17)(5.0)^{0.50} = 2.62,$$

under the assumption that the Sherwood number is a function of the Reynolds number to the 0.50 power for flow through stacked screens.[35] The observed increase in the limiting current density, from Fig. 11, is 4.8/2.5 = 1.93, off by a factor of 26%, which is not unreasonable if we consider the uncertainty involved in estimating the viscosity changes of the 20% KOH solution from 25°C to 57°C. In this case such a viscosity was assumed to change by the same factor that an equal molarity solution of NaOH does, since experimental viscosity data are available for NaOH solutions at different temperatures and higher concentrations than for KOH.

Effect of Solution pH

The effect of solution pH on the electroreduction of oxygen was studied in both platinum- and silver-screen electrodes. Runs on platinum screens were performed essentially throughout the whole available pH range, from pH = 0.55 to pH = 14.85. On the silver-screen electrode, the experiments were confined to the alkaline range because silver is attacked by acid solutions.

The results for the experiments on platinum screens are shown in Fig. 12 for pH = 10.1, in Fig. 13 for pH = 8.25, in Fig. 14 for pH = 1.85, and in Fig. 15 for pH = 0.55. These results clearly indicate that as the pH of the solution decreases, the electrochemical reduction of oxygen takes place with increasing difficulty. The electrode overpotential increases as the pH is lowered, and the slope of the Tafel line increases also. In acid solutions (pH values, 1.85 and 0.55) the voltage-logarithm of the current-density curves shows a gentle downward curvature that suggests an increase in the overall activation energy with increasing current densities. This phenomenon can be explained if we postulate that at higher current densities, the oxygen chemisorption rate on the electrode surface is limiting. It is a well-known fact that sulfate ions tend to chemisorb strongly on platinum electrodes in acid solutions.[13] These sulfate ions are blocking off sites that would otherwise be available to catalyze the oxygen-electroreduction reaction.

Figure 16 shows the same data plotted as electrode overpotential versus pH. The virtue of this manner of presenting the results is that the electrode "reversibility" can be appreciated at a glance. It becomes apparent that the oxygen electrode performance does not deteriorate very seriously until a pH of around 9 is reached, in platinum electrodes.

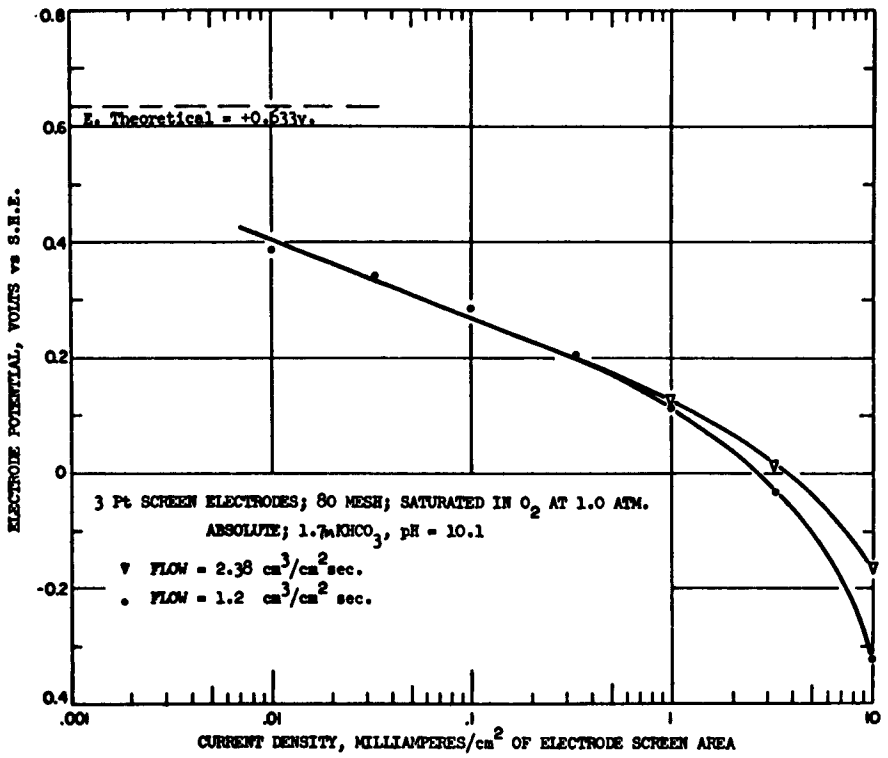

Fig. 12. Oxygen electroreduction on platinum at pH = 10.1.

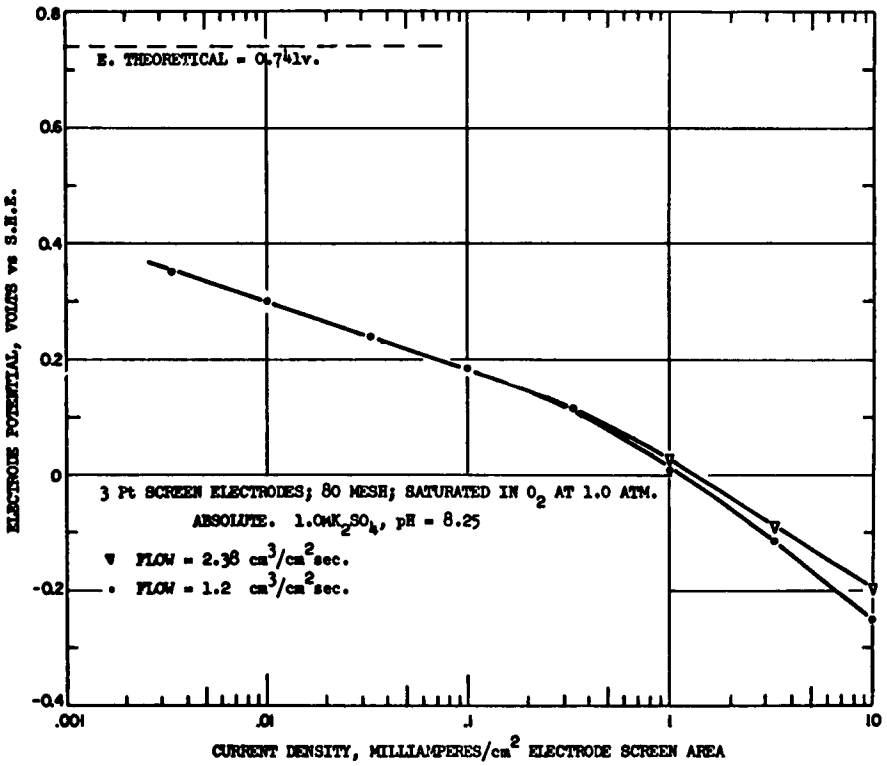

Fig. 13. Oxygen electroreduction on platinum at pH = 8.25.

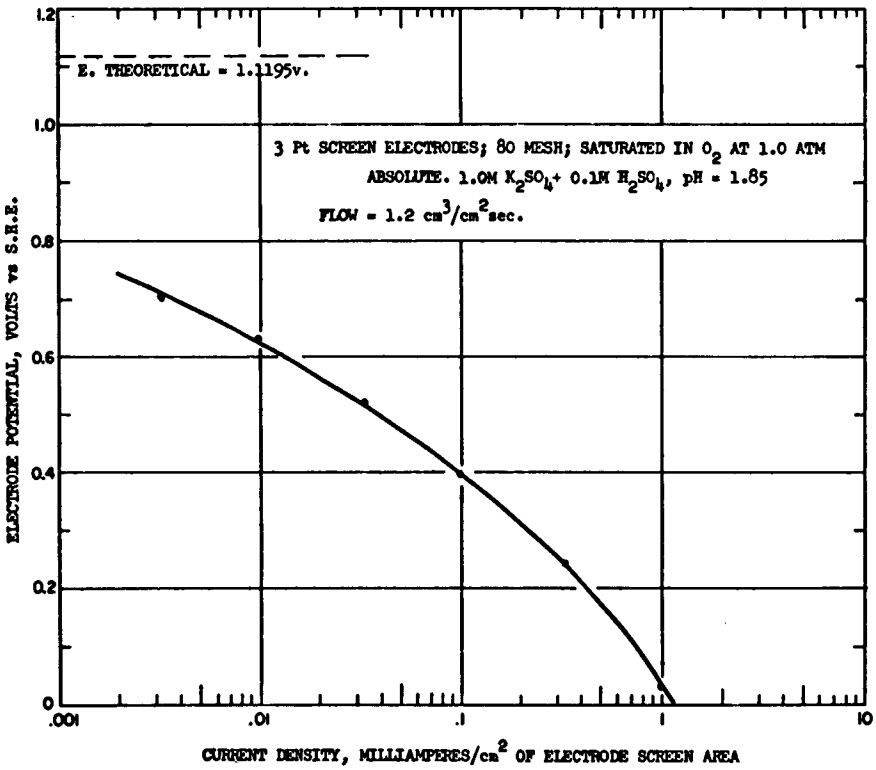

Fig. 14. Oxygen electroreduction on platinum at pH = 1.85.

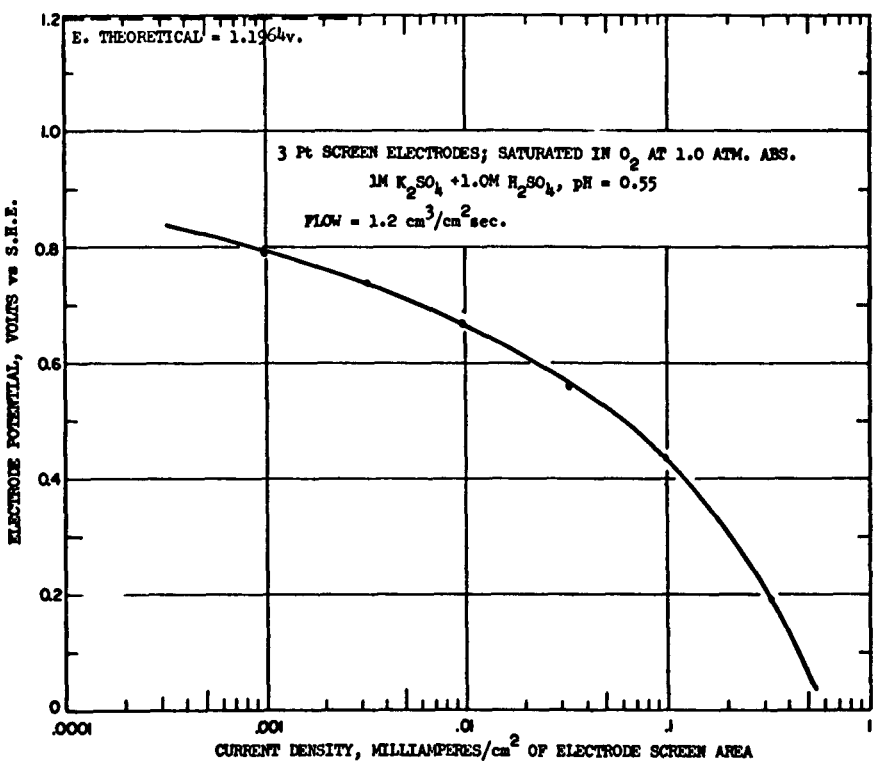

Fig. 15. Oxygen electroreduction on platinum at pH = 0.55.

The effect of solution pH on the electroreduction of oxygen on silver electrodes has been studied for pH values of 14.85, 11.5, and 10.1. The results of these runs are presented in Figs. 16, 17, and 18, and it is evident that they are of the same nature as the results obtained on platinum-screen electrodes. The overvoltages at current densities of interest (10^{-2} milliamperes per square centimeter, or higher) are so high as to indicate that there is not much hope for the operation of a practical oxygen electrode in other than basic solutions, with the catalyst materials investigated.

b. Hydrogen Peroxide Electroreduction

The results of the experiments for investigating the mechanism of hydrogen peroxide electroreduction are presented in Figs. 19, 20, and 21 for silver-screen electrodes, and in Figs. 22-26 for platinum-screen electrodes, and cover a wide pH range. These results are plotted as electrode potential (vs S.H.E.) vs log current-density curves, and, for the purpose of comparison, runs with the same electrolyte saturated in oxygen at 1.0 atm partial pressure, without any H_2O_2, are also shown. The hydrogen peroxide concentrations studied ranged between 0.001M and 0.1M. All runs were performed at 25°C.

There are several characteristics of the hydrogen peroxide electroreduction reaction that are common to all of the runs. First, the "open-circuit" potential of these electrodes is different from the open-circuit potential of the oxygen electrode, thereby indicating that H_2O_2, HO_2^- ions, or an adsorbed species of either, participates in the electrochemical reaction itself, which is different from the oxygen-electrode reaction studied above. Second, until moderate-to-high current densities are reached (10 ma/cm^2 on silver, 0.1M H_2O_2 in 20% KOH; or 0.2 ma/cm^2 on Pt, 0.1M H_2O_2 in 1M H_2SO_4) the electrode potential is constant and equal to the "open-circuit" potential, thereby indicating that this electrode reaction has a high exchange current density throughout the pH range. Such is not the case for the oxygen electroreduction reaction, and this explains why at low current densities the electrode potential corresponding to that of the H_2O_2 system is observed even if oxygen is present in the solutions, since the oxygen-electrode reaction is masked under this much faster reaction.

The hydrogen peroxide electroreduction reaction takes place quite irreversibly, as may be observed from comparison of the reversible calculated electrode potentials with the actual potentials. The electroreduction of 0.1M H_2O_2 in 20% KOH at 25°C has a reversible electrode potential

$$HO_2^- + H_2O + 2e^- = 3\ OH^- \qquad E^o = +0.88\ v \quad \text{(from Latimer)}.$$

In 20% KOH, $(OH^-) = 5.68$, and $(HO_2^-) \approx 0.1M$, since the ionization constant for H_2O_2 is 2.4×10^{-2}.

$$E_{rev} = E^o - \frac{RT}{nF} \ln \frac{(OH^-)^3}{(HO_2^-)(H_2O)}$$

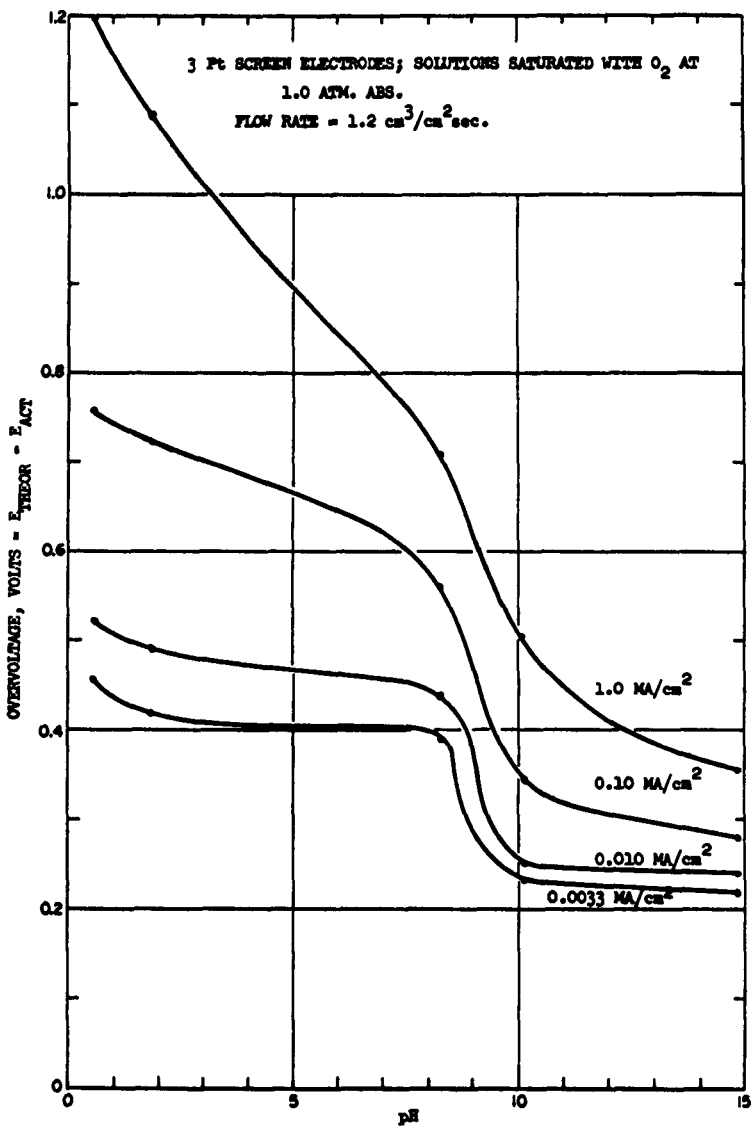

Fig. 16. Oxygen electroreduction overvoltage on platinum electrodes.

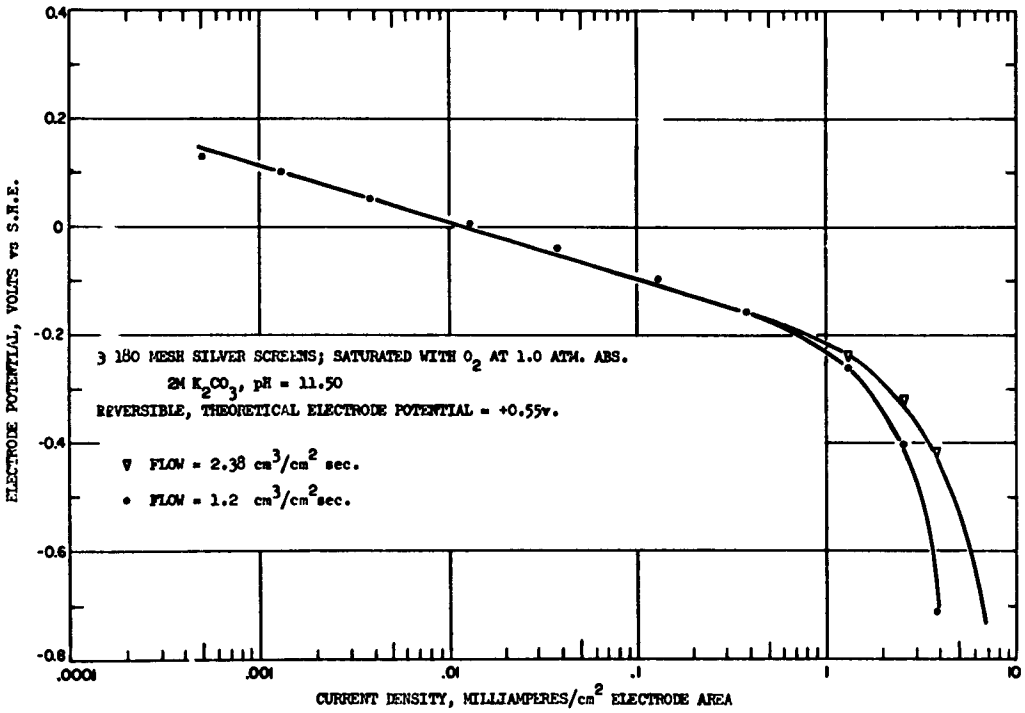

Fig. 17. Oxygen electroreduction on silver at pH = 11.50.

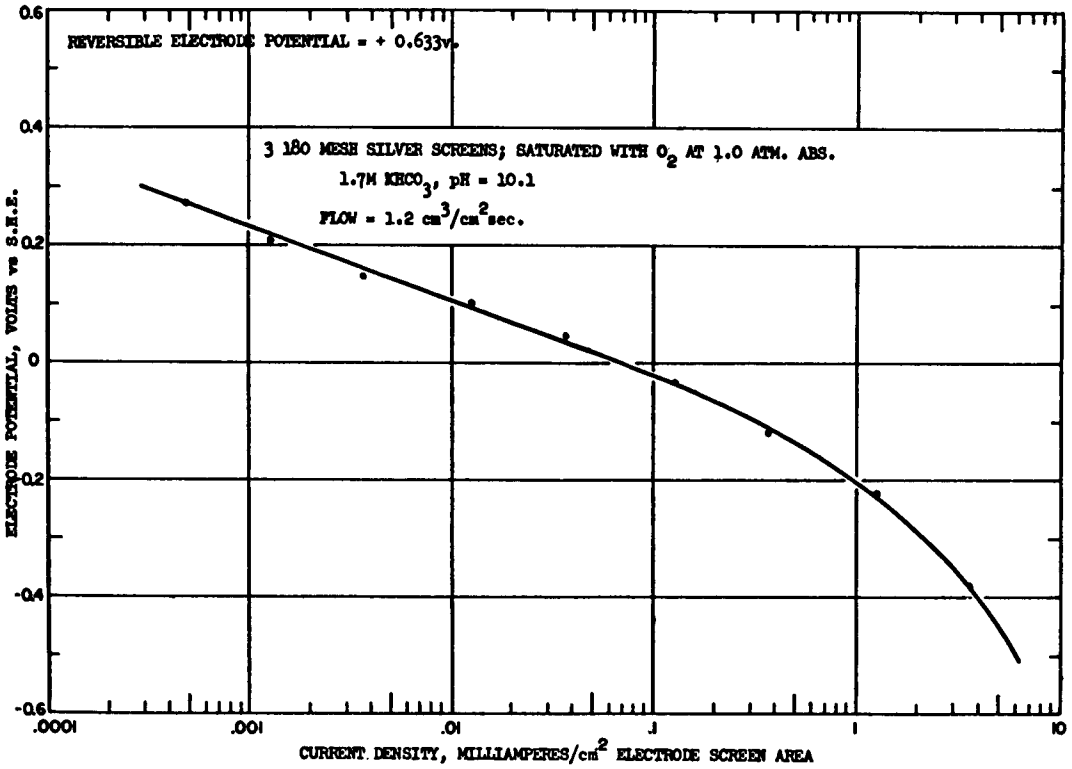

Fig. 18. Oxygen electroreduction on silver at pH = 10.1.

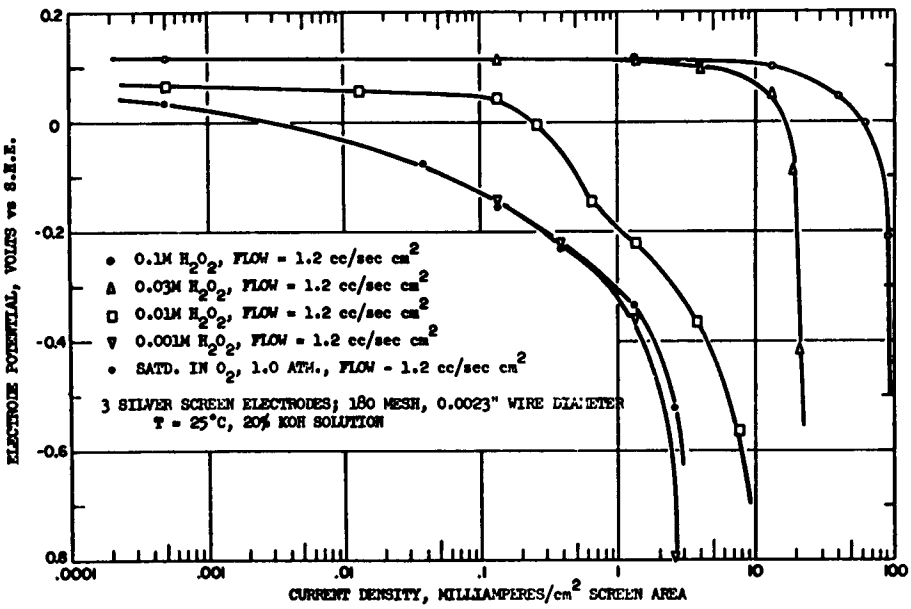

Fig. 19. Hydrogen peroxide electroreduction on silver in 20% KOH.

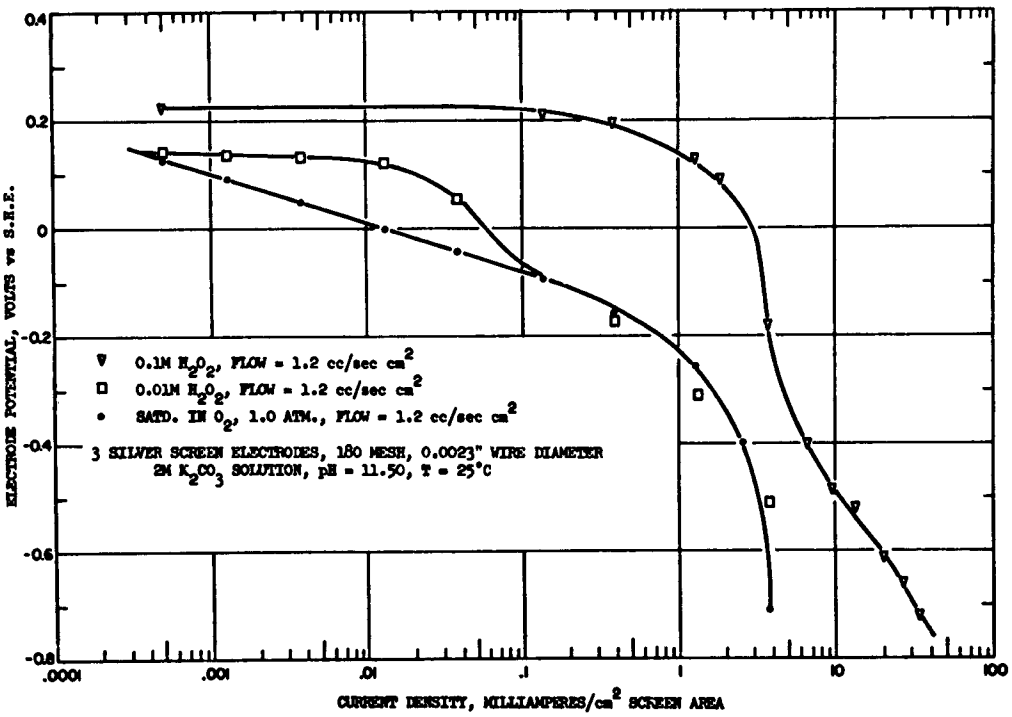

Fig. 20. Hydrogen peroxide electroreduction on silver at pH = 11.50.

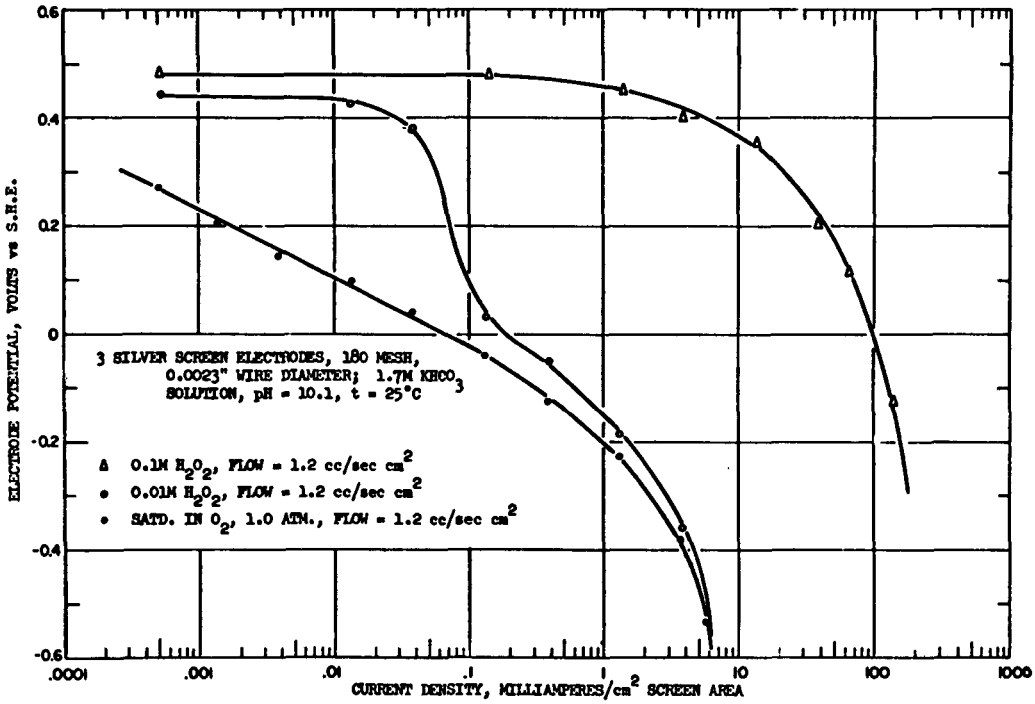

Fig. 21. Hydrogen peroxide electroreduction on silver at pH = 10.1.

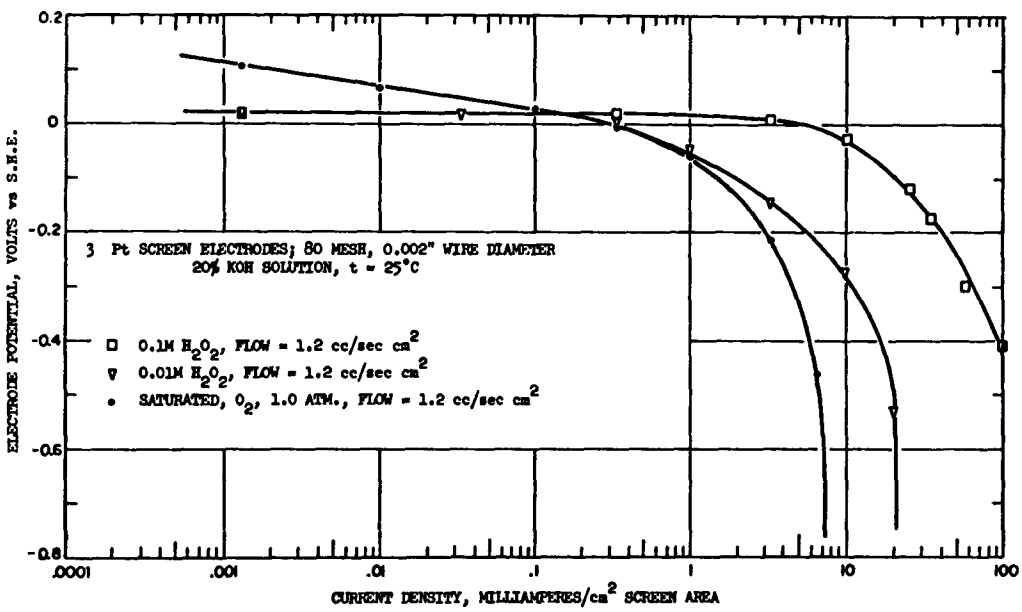

Fig. 22. Hydrogen peroxide electroreduction on platinum in 20% KOH.

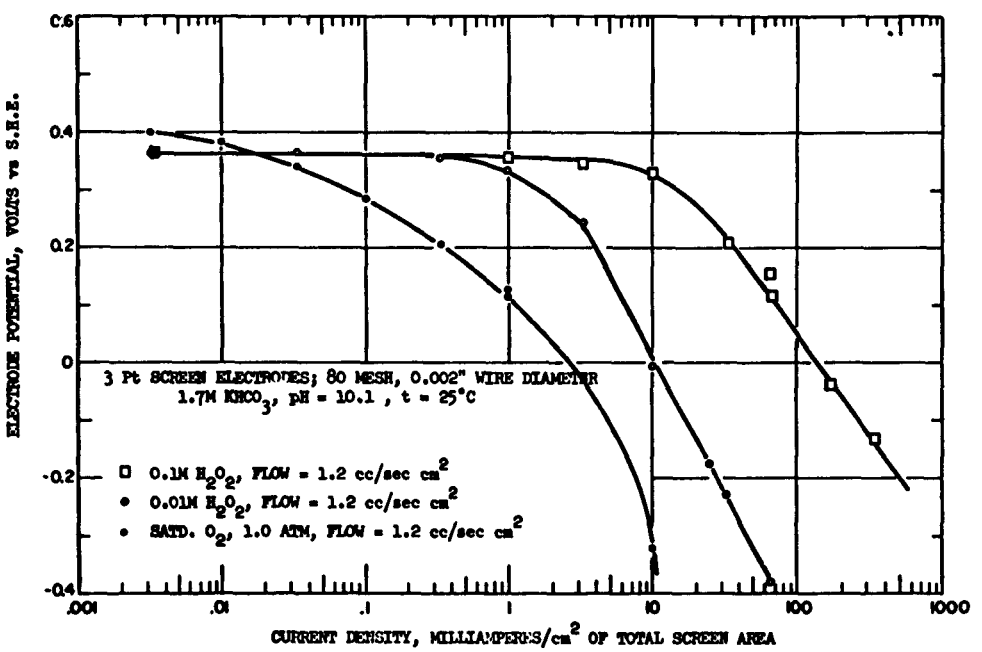

Fig. 23. Hydrogen peroxide electroreduction on platinum at pH = 10.1.

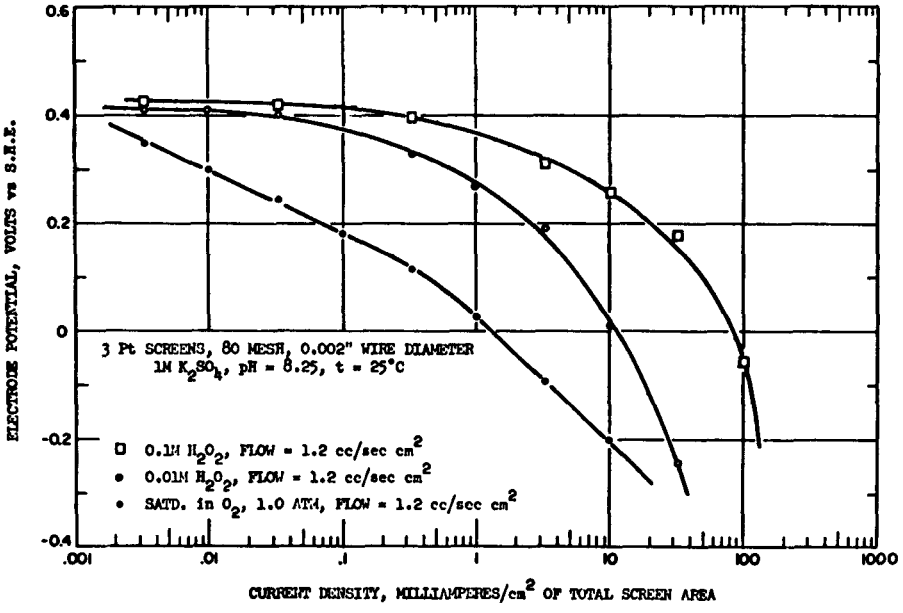

Fig. 24. Hydrogen peroxide electroreduction on platinum at pH = 8.25.

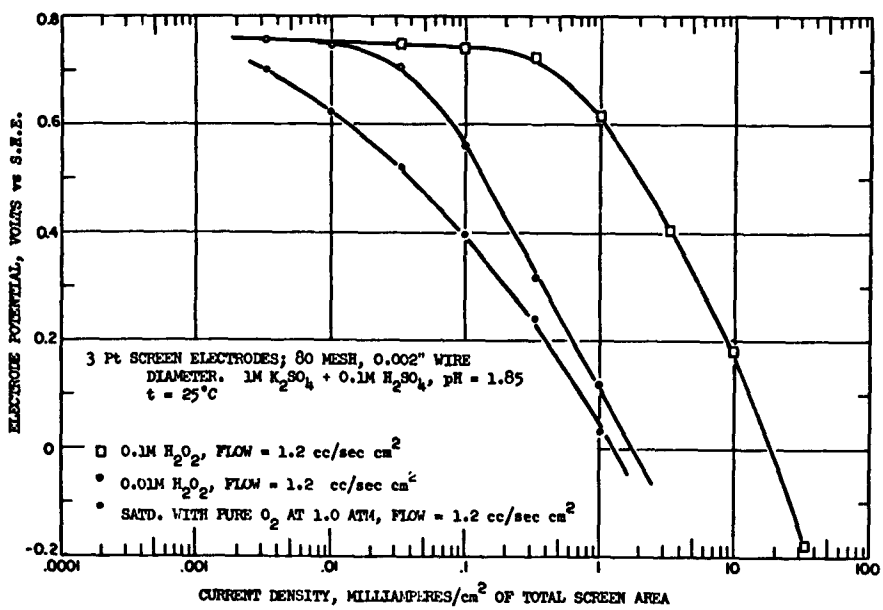

Fig. 25. Hydrogen peroxide electroreduction on platinum at pH = 1.85.

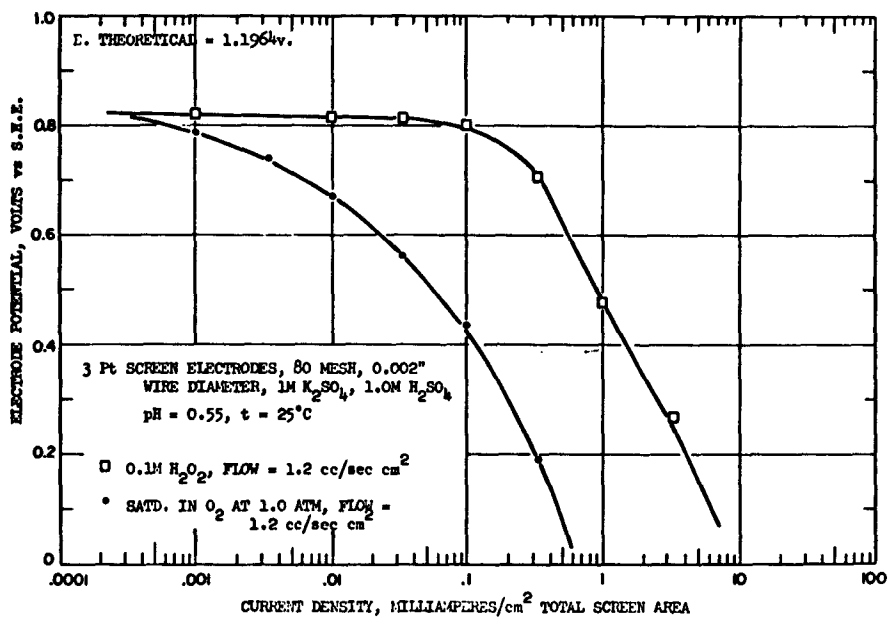

Fig. 26. Hydrogen peroxide electroreduction on platinum at pH = 0.55.

$$E_{rev} = 0.88 - 0.03 \log \frac{5.68^3}{0.1} = 0.785 \text{ volt}$$

Observed electrode potential: +0.02 volt in Pt (Fig. 22)
+0.12 volt in Ag (Fig. 19)

Thus the observed potential is 0.76 to 0.66 volt below the theoretical.

Similarly, in acid solution we calculate the reversible H_2O_2 electrode potential to be +1.707 volts (1M H_2SO_4 solution). The observed electrode potential for this solution is only +0.82 volt on a platinum-screen electrode (Fig. 26), or again approximately 0.9 volt below the reversible value. It should be noted that the observed hydrogen peroxide electroreduction potential is always even below the theoretical oxygen-electrode potential. One possible explanation for this high irreversibility is that the species that is being electroreduced is a strongly chemisorbed peroxy compound, and the high overvoltages observed correspond to the free energy lost during the irreversible chemisorption step.

Simultaneously with the hydrogen peroxide electroreduction reaction, a certain fraction of the hydrogen peroxide decomposes spontaneously at the electrode surface through the reaction

$$H_2O_2 \longrightarrow \frac{1}{2} O_2 + H_2O.$$

This spontaneous decomposition occurs more readily in basic than in acid solutions, and is strongly catalyzed by metals like silver, platinum, and so forth. This reaction has been studied in detail by Satterfield and co-workers.[36] The consequence of this reaction is that oxygen is present right at the electrode surface, and it can be reduced to water by the reaction described above.

As the hydrogen peroxide concentration in the solution is decreased, in all cases the limiting current density decreases too, but it is never smaller than the limiting current density for an oxygen electrode at 1.0 atm pressure, since at high enough overvoltage the oxygen electroreduction reaction takes over. This situation can be most clearly observed in Figs. 20 and 21, in which the voltage vs current-density curves for dilute peroxide solutions can be seen to meet the oxygen-electroreduction curves, and then follow along with them, thereby indicating that the oxygen electroreduction is now the predominant electrochemical reaction.

From all of these results, it is apparent that the hydrogen peroxide electroreduction reaction has no direct connection with the oxygen electroreduction reaction, and thus must be considered in its own light.

c. Hydrogen Oxidation Studies

Results of the experiments for studying the electrolytic oxidation of dissolved hydrogen in basic and acid solutions are presented in Figs. 27 and 28.

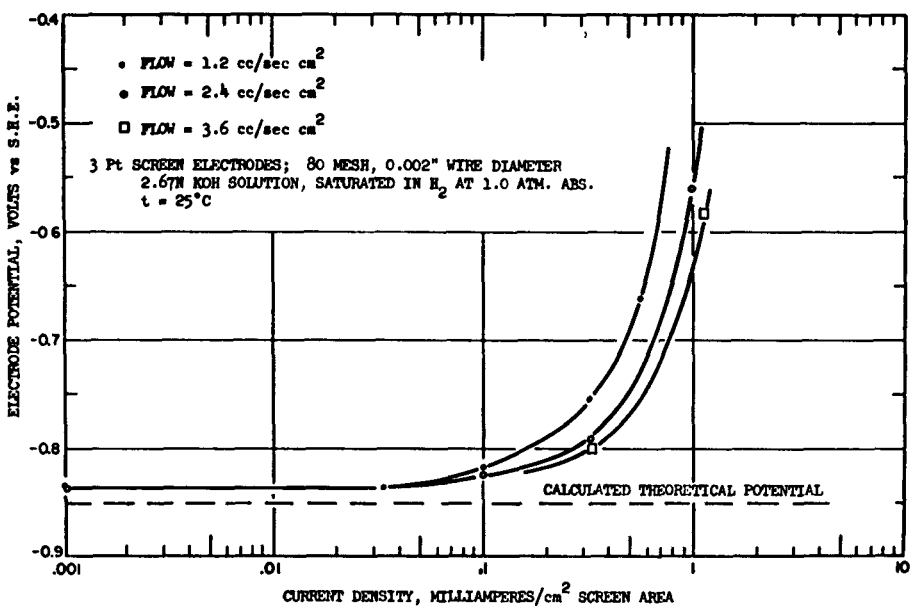

Fig. 27. Hydrogen electro-oxidation on platinum in 2.67 N KOH.

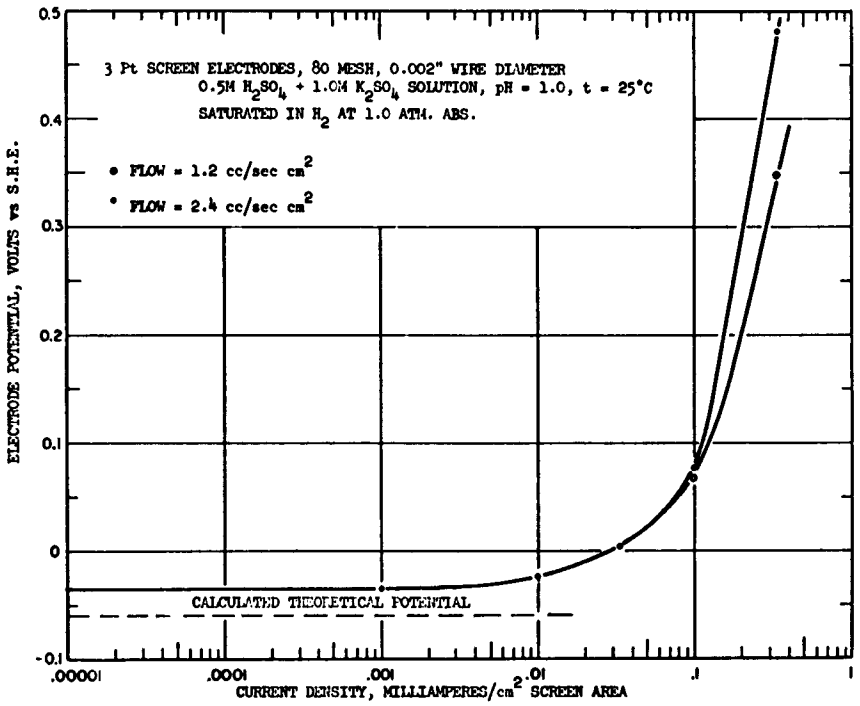

Fig. 28. Hydrogen electro-oxidation on platinum at pH = 1.0.

It can be observed from these results that in both cases the electrode potential is constant and equal to the open-circuit potential up to fairly high current densities (0.05 ma/cm^2 in base, and 0.01 ma/cm^2 in acid). This fact is consistent with the observations of other authors that the hydrogen-electrode reaction does have a high exchange-current density, of the order of 10^{-4} amp/cm^2. The reversibility of the hydrogen electrode in this low-current-density region is evident from comparison of the observed electrode potentials with the calculated reversible potentials for both solutions: in basic solution the observed potential is within 12 mv of the theoretical potential, and in acid solution the difference is only 24 mv. Such a difference is within the limits of the experimental error, if we consider that the calomel reference electrode potential is known only within 20 mv, because of liquid-junction potential effects that are not taken into account in this work.

As the current density is increased, a region is reached where the hydrogen-electrode potential is dependent on the hydrogen-supply conditions (hydrogen concentration and saturated electrolyte flow rate), just as in the oxygen-electrode studies. The limiting current densities are of the order of magnitude expected from mass-transfer calculations; therefore we see that hydrogen concentration polarization is responsible for the final sharp rise in potential. Again, as in the case of the oxygen electrode, the transition from pure electrochemical kinetics governing the electrode potential to concentration polarization is not as sharp as would be expected from theory, if these were the only two phenomena taking place. These results suggest that the rate of hydrogen chemisorption on the platinum surface is influencing the electrode behavior, if we use the same arguments presented in the case of the oxygen electrode.

It is clear that the electrochemical kinetics per se is not limiting the electrode performance. Furthermore, the electrochemical kinetics for this reaction has been studied in great detail by many authors, and emphasis on this type of study is not necessary. From the results obtained, however, it appears that in order to calculate the hydrogen-electrode performance more must be known about the rate of hydrogen adsorption on the electrode surface, and its influence on electrode performance. Such a study was not possible for the present work because it was not possible to vary the hydrogen partial pressure through a wide enough range, mainly at pressures above 1 atmosphere, to yield useful results.

d. Ethylene Oxidation Studies

Experiments directed toward the investigation of the electrochemical oxidation of ethylene on platinum screens in 1M $KHCO_3$ and 0.5M H_2SO_4 solutions were performed. We found that this reaction takes place with such difficulty in both cases that no reliable data could be obtained. High polarizations were encountered at current densities of approximately 0.1 μamp per square centimeter, and thus any study of this electrode process should be conducted in an experimental system in which the presence of even traces (10^{-10} g moles/cc) of oxygen is eliminated. The experimental system used was

not suited to this type of operation.

At any rate, an electrochemical reaction that takes place with such difficulty is not of practical interest, and all efforts concerning an ethylene electrode should be directed toward the improvement of the catalytic system itself, and not on performance studies of the present system.

3.3 CALCULATIONS OF ELECTRODE PERFORMANCE FROM EXPERIMENTAL DATA

With the electrochemical kinetic data given in section 3.2, it is possible to undertake electrode performance calculations for the systems studied. We decided to perform these calculations for the oxygen-electrode system, since it is of greater practical interest, and its kinetics has been most thoroughly studied.

The oxygen electroreduction kinetics on a platinum catalyst material in a 20% KOH solution is summarized in Fig. 5. It can be seen that the current density is uniquely defined by only two variables in this system: the electrode potential, and the oxygen concentration (partial pressure) at the electrode surface. Therefore, if it is possible to calculate the oxygen concentration at every point within the electrode surface, at a given potential the current density can also be calculated, to yield an electrode-potential vs current-density curve (performance curve).

In calculating the performance of a porous gaseous-diffusion electrode, a basic electrode geometry must be settled upon. It is evident that this geometry must make as much electrode surface as possible available to catalyze the electrochemical reaction. Smooth platinum or silver at 25°C will support only enough electrochemical reaction for a current density of approximately 1 ma/cm^2 at 0.35 volt below the reversible potential, whereas current densities 100 to 1000 times as great are sought in fuel cells. Even if catalytic electrode surfaces capable of supporting such high current densities were available, they would be able to receive the necessary oxygen only when covered with electrolyte films of impractical thinness. For example, consider a flat plate of very active smooth electrode material covered by a stagnant layer of electrolyte. At 25°C, if oxygen at 1 atm is present on the outside of this film, then sufficient oxygen transport to support 500 ma/cm^2 will occur only if the electrolyte layer is thinner than 10^{-6} cm.

This limitation of the flat nonporous plate is overcome by the porous gas-diffusion electrode, which makes possible the attainment of high current densities per unit face area, even though diffusional resistance to mass transfer is great, and specific activity of the catalyst surfaces is not high. That is, these porous electrodes provide an enormous amount of surface in the immediate vicinity of the gas-liquid interface, so that even with a low specific current density, relatively high current densities per unit electrode face area are obtained. There are, however, practical limitations to the diameter and maximum number of micropores that can be accommodated. There is a minimum pore diameter of approximately 30 Å set by the dimensions of the molecules

and hydrated ions that are being transported. Furthermore, there is a minimum spacing between pores set by structural considerations which fixes the maximum number of pores present.

Recognizing these limitations, it is possible for us to calculate the theoretically attainable performance of various electrode structures. Assume that the electrode is a flat plate containing a multiplicity of cylindrical pores, somewhat along the lines of Austin[1] as shown in Fig. 1. These pores are at right angles to the electrode face, are evenly distributed with a distance of two diameters from center to center, and assumed to be filled with liquid so that the gas-liquid interface lies somewhere within the pore. The adoption of such an idealized geometry simplifies the calculations, but still gives results that are quite applicable to less uniform geometries.

In order to calculate the total amount of oxygen that is being reduced throughout the pore at a given overvoltage, the pore wall can be treated as an equipotential surface; this is a good assumption as the electrode material (platinum or silver in this case) is a good conductor. The current density at any point within the pore will be determined by the oxygen concentration at that point, and this concentration can be obtained by a finite differences calculation throughout the pore, starting at a point where essentially a very low oxygen concentration exists, and calculating step by step the concentration increases (and consequent current-density increases) as the pore mouth is approached. A typical calculation of this kind is presented in Appendix D.

The results of such an analysis for a porous system of 30 Å pore diameter, platinum catalyst surface, oxygen at 1 atm partial pressure at the pore mouths, and 60 Å pore spacing are shown in Fig. 29. This performance is not yet very attractive, hence the electrode model just presented must be revised to increase even further the amount of electrode surface available for electrochemical reaction. By use of macropores from each of which the small micropores radiate, the number of micropores per unit of electrode face area increases greatly. Such a geometry is sketched in Fig. 30. In considering the spacing, diameter, and depth of these macropores, the following factors are relevant:

(a) The interpore wall thickness should be approximately twice the "active length" of the micropores, so that all micropores can function properly.

(b) Liquid penetration into the porous structure should be small enough to avoid large IR drops within the electrolyte in the pores.

The first consideration determines the diameter of the macropores to be approximately 4 microns, since from the calculation outlined above it is found that appreciable reaction occurs within the micropores for a length of approximately 2 microns. For the case under consideration, the resistivity of 20% KOH at 25°C is 2 ohm-cm. In the given geometry, the porosity of the solid microporous structure will be

$$\epsilon = \frac{\pi d^2}{4(2d)^2} = 0.196.$$

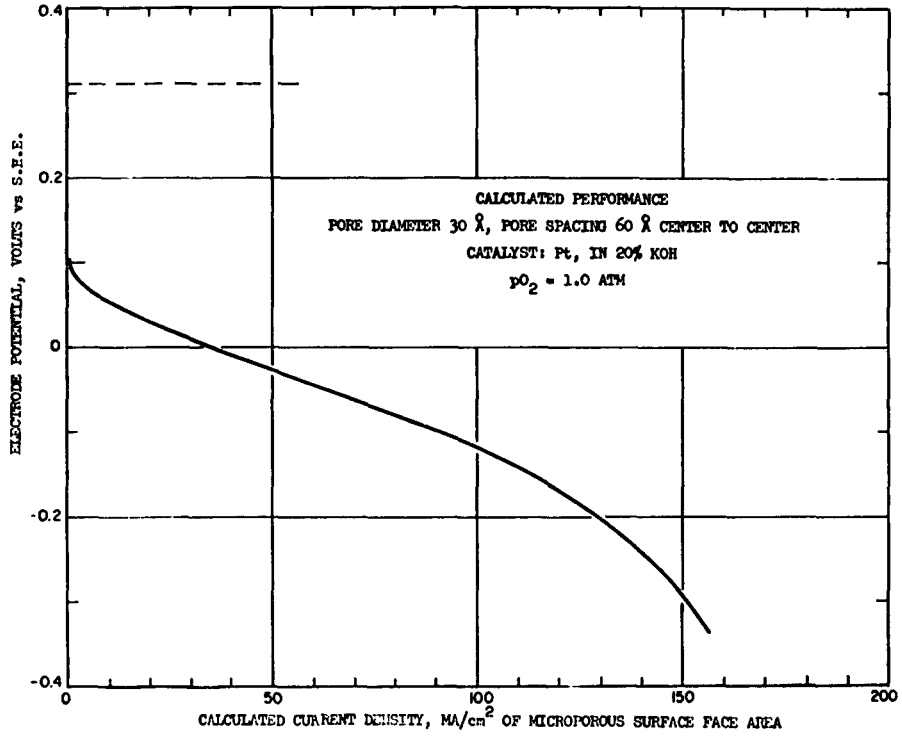

Fig. 29. Calculated performance for a 30 Å micropore surface.

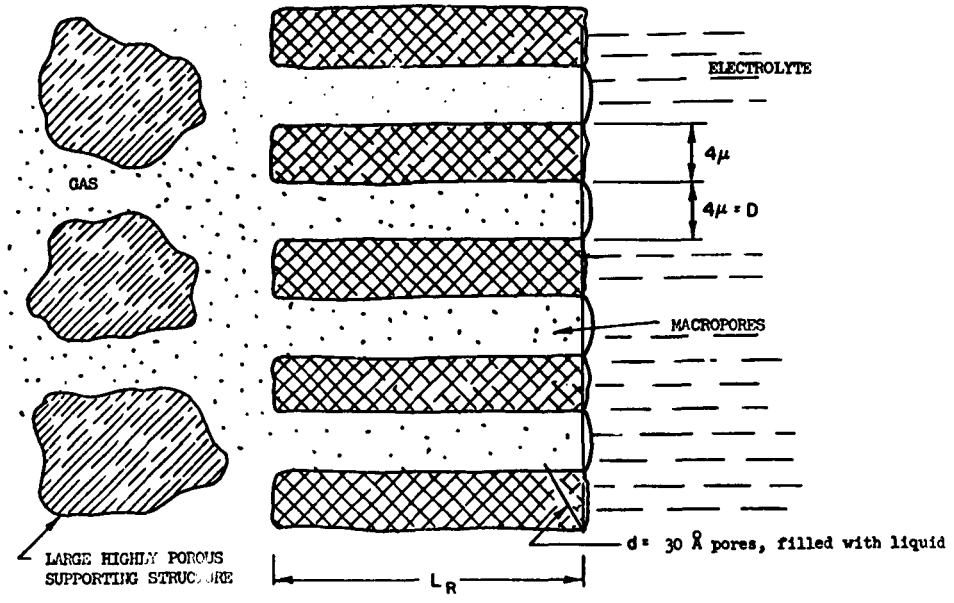

Fig. 30. Combination of microporous and macroporous structures.

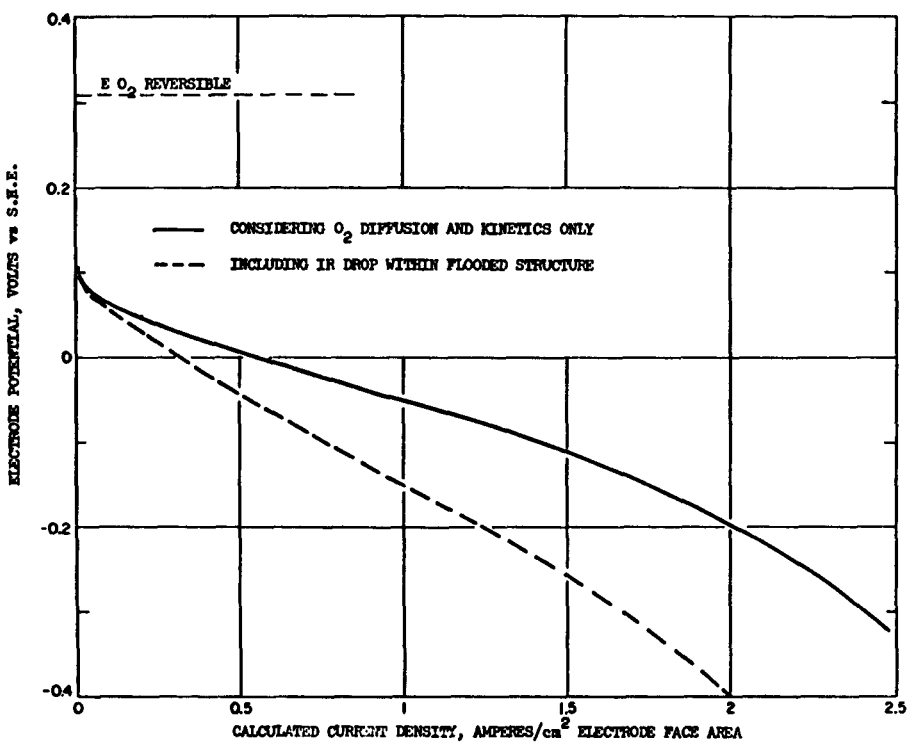

Fig. 31. Calculated performance for the microporous-macroporous structure of Fig. 30.

Since the micropores in an actual case are not straight, a tortuosity path q of approximately 2 (a typical number for porous systems) may be considered. The effective resistivity[1] of the flooded microporous material is

$$\rho'_{eff} = \rho'_{free}\frac{q}{\epsilon} = \frac{(2)(2)}{0.196} = 20.4 \text{ ohms-cm.}$$

The resistivity of the layer as a whole, if we take into account the existence of nonconducting, nonflooded macropores (the tortuosity path factor here will be negligible, since the "flooded solid" occupies approximately 80% of the total volume) is

$$\rho' = \frac{20.4}{(1-0.196)} = 25.4 \text{ ohms-cm}$$

if the macropores are spaced two diameters from center to center as well.

If we consider a reasonable IR drop within the electrode to be 0.1 volt at 1.0 amp/cm^2 of electrode face area, the thickness of this active layer will be

$$L_R = \frac{2(\Delta V)}{I_F R} = \frac{2(0.1)}{1.0(25.4)} = 0.00786 \text{ cm,}$$

under the assumption that the current is nearly uniformly generated throughout the macropore.

The face area of the flooded microporous material per unit electrode face area will then be

$$\frac{\text{number of macropores}}{\text{cm}^2 \text{ electrode face area}} \text{ (effective area of macropore)}$$

$$= \frac{\pi DL}{4(2D)^2} = \frac{\pi(0.00786)}{4(4)\ 10^{-4}} = 15.5 \text{ cm}^2/\text{cm}^2.$$

The calculated electrode current density per unit electrode face area for the micro-macropore structure is shown in Fig. 31. The lower performance curve of Fig. 31 incorporates the effect of the IR drop through the flooded micropore area.

This calculated performance curve has the same general shape as the experimental curve obtained for porous gas-diffusion electrodes by many investigators.[7,37] One interesting point is that the calculated performance for this system, which has not been optimized, is higher than any electrode performances yet observed. This means that by building an electrode of the appropriate geometry, higher electrode performances than the ones at present observed should be attained. The calculations above also show the relative influence of the different operating and geometrical variables on electrode performance, and should be helpful in determining the optimal configuration for any given electrode system and operating conditions.

IV. CONCLUSIONS

The conclusions resulting from this investigation can be divided into two groups, one concerning findings on the electrode-kinetics studies, and the other referring to findings connected with the electrode-performance studies.

4.1 ELECTRODE KINETICS

For all electrodes studied, we found that for a given solution-electrode system, the electrode potential is uniquely determined by the reactant and reaction product concentration at the electrode surface, and the electrode current density.

The experimental method employed in these studies (flowing a reactant-saturated electrolyte past an electrode of known geometry) is particularly suited to the study of these specific reaction rates as a function of current density and reactant concentration, since from it reproducible and readily interpretable results can be obtained on the basis of current density per unit of actual electrode area.

a. Oxygen Electroreduction Reaction on Platinum and Silver

At very low current densities (10^{-7}-10^{-4} amp/cm^2) the electroreduction kinetics is the sole process that controls the electrode potential. In the current-density range of practical interest (10^{-4}-10^{-2} amp/cm^2), however, the oxygen chemisorption step is rate-limiting, and this results in abnormally high overvoltages (premature deviation from the Tafel line).

The oxygen electroreduction rate on platinum and silver electrodes decreases at a given overpotential as the solution pH is decreased. This change is most pronounced at a pH value of approximately 9.

b. Hydrogen Peroxide Electroreduction

The hydrogen peroxide electroreduction reaction has a high exchange-current density (from 10^{-2} amp/cm^2 to 2×10^{-4} amp/cm^2, which depends on the conditions), and very high specific current densities (up to 10^{-1} amp/cm^2 in 0.1M H_2O_2-20% KOH) can be obtained, with the electroreduction kinetics being the sole rate-controlling step at all times. There is no evidence that a chemisorption step is rate-controlling even at the highest current densities.

Since the hydrogen peroxide decomposes spontaneously at the electrode surface through the reaction

$$H_2O_2 \longrightarrow \tfrac{1}{2} O_2 + H_2O,$$

the oxygen electroreduction reaction takes place concurrently with the hydrogen peroxide electroreduction, and, in some cases, becomes the potential determining reaction.

c. Hydrogen Electro-oxidation

As other investigators have observed, the hydrogen electrode reaction is essentially reversible at low current densities, the open-circuit potential being equal to the theoretical reversible electrode potential. The exchange-current density for the hydrogen electrode reaction on platinum is high, of the order of 10^{-4} amp/cm^2, and thus electrochemical kinetics is not expected to be limiting under most circumstances.

In the current-density range of practical interest (10^{-2}-10^{-4} amp/cm^2) the hydrogen chemisorption step is rate-limiting, resulting in abnormally high overpotentials.

d. Ethylene Oxidation

The electrochemical oxidation rate of ethylene on platinum electrodes in 1M $KHCO_3$ and 0.5M H_2SO_4 solutions was found to be impractically low, resulting in high electrode polarization at current densities as low as 10^{-7} amp/cm^2. The electrode kinetics in this case is controlling the electrode potential at all times.

4.2 ELECTRODE-PERFORMANCE STUDIES

(i) The performance of a gaseous-diffusion electrode of idealized geometry can be calculated if the electrode kinetics is known as a function of electrode potential and reactant concentration.

(ii) In order to achieve satisfactory electrode performance, an electrode containing both electrolyte-flooded micropores (30-100 Å in diameter) and nonflooded macropores (1-10 microns in diameter) is necessary, in order to maximize the amount of electrode active area per unit of electrode face area.

(iii) In order to keep the ohmic drops within the electrode down to a reasonable value, the thickness of this "active" flooded micropore region must be of the order of 10^{-2} cm.

(iv) If such an idealized geometry is achieved, it should be possible to greatly increase the performance of gaseous-diffusion oxygen electrodes above the best performance that has been achieved thus far with the available catalyst materials.

V. RECOMMENDATIONS FOR FURTHER RESEARCH

On the basis of the findings made during this investigation, the following recommendations can be made in connection with further fuel-cell electrode research.

(i) Any electrode-kinetic studies directed toward oxygen or hydrogen electrode design or performance calculations should take into consideration the strong role played by the reactant chemisorption step in controlling the electrode-performance curve. The effect of a wide range of reactant concentrations at the electrode surface should be studied, to determine more quantitatively the limitations imposed by the chemisorption rate of the reacting species.

(ii) The development of a gaseous-diffusion electrode of a geometry similar to the one described in Fig. 30 should be undertaken, and the performance of such an electrode should be checked against the predicted performance.

APPENDIX A

LIMITING CURRENT-DENSITY CALCULATIONS FOR FLOODED SCREENS

A.1 Stoichiometric Limiting Current Densities

It is clear that the screen electrodes cannot electroreduce more oxygen than the amount that is supplied dissolved in the electrolyte. The following calculation shows the magnitude of the obtainable current densities if all of the oxygen were to be consumed, for flow conditions typical of most of the runs that were performed. These calculations permit a quick evaluation of the fraction of the total oxygen consumed in each run.

Case 1.

Flow rate = 1.2 cc/cm^2 screen face area second (as in curve 2, Fig. 5).

Solution: 20% KOH (4 moles per liter) saturated in O_2 at 1.0 atm.

Solubility of O_2 = 2.9×10^{-7} g moles/cc atm[38] by Fig. 32.

I_L = (1.2 cc/cm^{2}sec)(2.9×10^{-7} g moles/cc)(4)(96,500 coulombs/g mole)

= 0.134 amp/cm^2 electrode face area.

Case 2.

Flow rate = 2.4 cc/cm^2 screen face area second (as in curve 3, Fig. 5).

Other conditions are the same as in Case 1.

I_L = (2.4)(2.9×10^{-7})4(96,500) = 0.268 amp/cm^2

A.2 Mass-Transfer Calculations for Screens

Since no mass-transfer data are available for screens of this particular geometry, the mass-transfer coefficients can be approximated by calculating the mass transfer for flow normal to a cylinder of the screen wire dimensions. The calculations are performed for the 20% KOH runs at 25°C. The fluid properties are tabulated as follows:

μ = 10 lb/hr ft

C_p = 0.85 Btu/lb °F

k = 0.35 Btu/hr ft^2 °F/ft

D_L = 1.79×10^{-5} cm^2/sec

ρ = 70 lb/ft^3

Case 1.

Platinum screen, 80 mesh, 0.002-in. wire diameter.

Free-flow area = 1-2 (80)(0.002) = 0.680.

Solution saturated in O_2 at 1 atm, Flow = 1.2 cc/cm^{2}sec.

$$U_{ave} = \frac{U_{entrance} + U_{max}}{2} = \frac{1.2 + 1.2/0.680}{2} = 1.5 \text{ cm/sec}$$

$$N\,Re = \frac{D\,U_{ave}\rho}{\mu} = \frac{(0.002)(1.5)(70)3,600}{12(10)30.4} = 0.210.$$

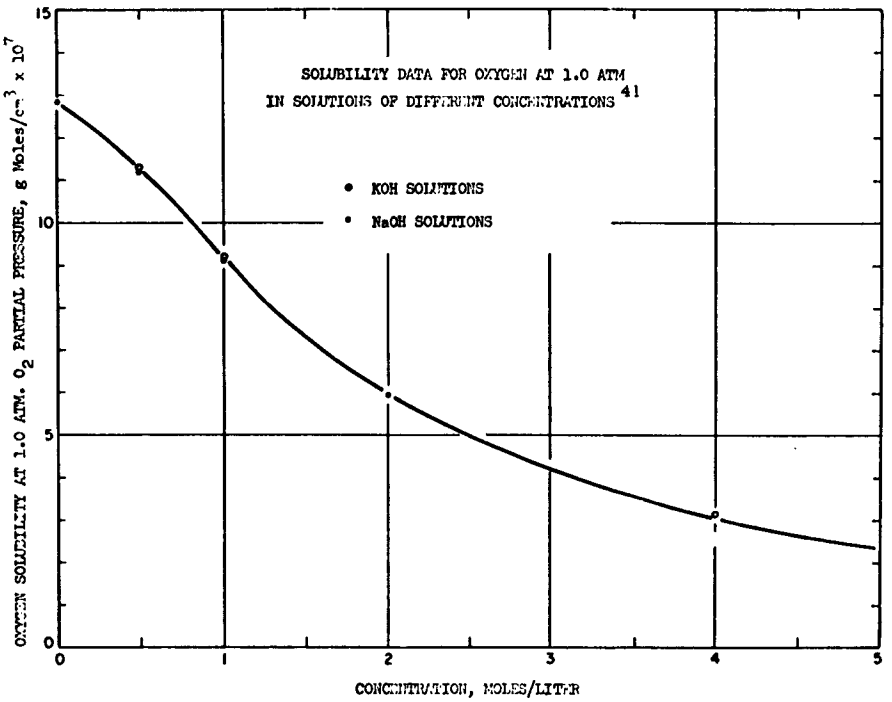

Fig. 32. Solubility data for oxygen at 1.0 atm in electrolyte.

From McAdams,[33] Figs. 10-12, $\frac{hD}{k}\left(\frac{C\rho\mu}{k}\right)^{-0.3} = 0.40$. Then the Nusselt number = $\frac{hD}{k} = 0.40(2.88) = 1.15$.

From the heat-mass transfer analogy, the Sherwood number will be

$$\frac{k_L D}{D_L} = \frac{hD}{k}\left(\frac{\mu/\rho D_L}{C\rho\mu/k}\right)^{1/3} = 1.15(85)^{0.33} = 5.1$$

$$k_L = \frac{5.1(1.79 \times 10^{-5})}{5.1 \times 10^{-3}} = 1.79 \times 10^{-2} \text{ cm/sec.}$$

The limiting current density, I_L, then is

$$I_L = \overrightarrow{N_A} nF = k_L(c_b - 0)\, nF$$

$$= 1.79 \times 10^{-2}(2.9 \times 10^{-7})4(96,500) = 2.0 \times 10^{-3} \text{ amp/cm}^2.$$

Case 2.

Same conditions as for Case 1, except that the solution is saturated in air (pO_2 = 0.21 atm).

$I_L = 2.0 \times 10^{-3}(0.21) = 4.2 \times 10^{-4}$ amp/cm^2.

Case 3.

Silver Screens, 180 mesh, 0.0023-in. wire diameter.

Free-flow area = 1-2(180)0.0023 = 0.174.

Solution saturated in O_2 at 1 atm, flow = 1.2 cc/cm^{2}sec.

$$U_{ave} = \frac{1.2 + 1.2/0.174}{2} = 4.05 \text{ cm/sec.}$$

$$N\,Re = \frac{0.0023(4.05)(70)(3,600)}{(12)(30.4)(10)} = 0.64.$$

From McAdams,[33] Figs. 10-12, $\frac{hD}{k}\left(\frac{C\rho\mu}{k}\right)^{-0.3} = 0.7$. Then the Sherwood number will be

$$\frac{k_L D}{D_L} = \frac{hD}{k}\left(\frac{\mu/\rho D_L}{C\rho\mu/k}\right)^{1/3}$$

$$= (0.7)(2.88)(5.1) = 10.3$$

$$k_L = \frac{10.3(1.79 \times 10^{-5})}{5.85 \times 10^{-3}} = 3.14 \times 10^{-2} \text{ cm/sec.}$$

The limiting current density is

$$I_L = \vec{N}_{O_2} nF = 3.14 \times 10^{-2}(2.9 \times 10^{-7})4(96,500) = 3.5 \times 10^{-3}\ A/cm^2.$$

Case 4.

Same conditions as for Case 3, except that the solution is saturated in air at 1 atm (pO_2=0.21 atm)

$I_L = 3.5 \times 10^{-3}(0.21) = 0.736 \times 10^{-3}$ amp/cm^2.

APPENDIX B

DOUBLE-LAYER CAPACITANCE CALCULATIONS

The equivalent circuit for the system consisting of test electrode, T and electrolyte dummy electrode, D can be approximated as

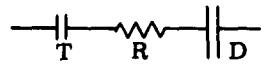

If the dummy electrode has a much larger surface area than the test electrode (in this case, 100 cm^2 as compared with 3.0 cm^2), the capacitance of the whole system will be equal to the capacitance of the test electrode, since

$$\frac{1}{C_s} = \frac{1}{C_T} + \frac{1}{C_D}.$$

The charging curve of the test-electrode electric double layer when a direct-current step (square wave) is applied, can be described by

$$C_T = I\left(\frac{dt}{dv}\right),$$

where I is the absolute magnitude of the current step, and dt/dv is the reciprocal of the slope of the charging curve. It is assumed that I remains constant as the electrode interfaces become charged. This is a good assumption if the impedance changes of the electrode system are small compared with the total impedance of the circuit opposite the signal generator. This is certainly the case in the present experiments, since the 10,000-ohm resistor in series with the electrode system (see Fig. 3) is much larger than the electrode system resistance (approximately 2 ohms).

The amplitude of the square-wave output from the signal generator was adjusted to 5.00 volts by means of the cathode-ray oscilloscope. The magnitude of the current step I then is

$$\Delta I = \frac{\Delta V}{R'} = \frac{5.0}{10,000} = 5 \times 10^{-4} \text{ amp.}$$

A typical picture of the output observed in the cathode-ray oscilloscope screen is presented in Fig. 33. The charging-curve slope for the upper picture (the straight-line portion) can be measured, and is found to be

$$\frac{dv}{dt} = 0.915 \text{ volt/sec.}$$

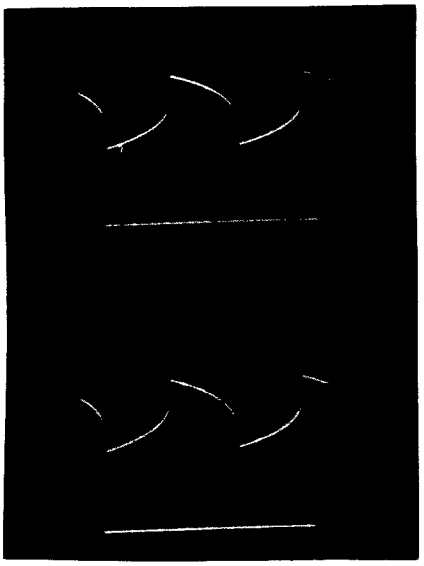

Charging-Curve Beam

Vertical axis, scale . . . . . 500 microvolts/cm

Horizontal axis, scale . . . . . 2×10^{-4} sec/cm

Electrode-Potential Monitoring Beam

Vertical axis, scale . . . . . 0.100 volt/cm

Horizontal axis, scale . . . . . 100 sweeps/sec

Calibration . . . . . 0.00 volt at bottom of scale

Fig. 33. Double-layer charging curves.

The measured capacitance then is

$$C_T = I\frac{dt}{dv} = 5 \times 10^{-4} \frac{1}{0.915} = 5.48 \times 10^{-4} \text{ farad.}$$

Since the test-electrode surface area is 3.0 cm^2, the electrical double-layer capacitance is

$$C_{DL} = \frac{5.48 \times 10^{-4} \times 10^6}{3.0} = 183 \ \mu fd/cm^2.$$

APPENDIX C

POROUS CARBON ELECTRODE PREPARATION

The Kordesh[39, 40] type of impregnated porous carbon electrode used in the experiments described in section 2.2a (Electrode No. 16) was prepared in the manner described below.

A 1.0-in. diameter, 0.25-in. thick, disk was machined out of a National Carbon Company, Grade 20, porous graphite block. This material has a porosity of 48%, and an average pore diameter of 140 microns. The disk then underwent treatment as follows:

1. Washed in benzene,
2. Dried in 110°C oven for 1.0 hour,
3. Washed in 30% HNO_3 for 5 minutes,
4. Dried in 110°C oven for 1.0 hour,
5. Impregnated with the catalyst metal's solution (fully immersed to soak),
6. Dried in 110°C oven for 1.0 hour, and
7. Baked in H_2 furnace at 850°C for 1.0 hour, cooled in the same H_2 atmosphere to room temperature.

The composition of the catalyst metal's impregnating solution was

100 cc Distilled Water

5.65g $AgNO_3$

12.50g $Al(NO_3)_3$

which yielded a metal loading of the electrode

1.7% by weight Ag

1.76% by weight Al.

The aluminum was then leached out in strong caustic. No attempt was made to find out how the metal was distributed throughout the electrode.

APPENDIX D

CALCULATIONS OF THE TOTAL CURRENT WITHIN A PORE

Choose a pore diameter, say, 30 Å, and material Pt.

Oxygen partial pressure at the pore mouth, 1.0 atm.

From Fig. 5, on a platinum electrode in 20% KOH, the oxygen electroreduction rates can be read. At an electrode potential of 0.00 volt vs the S.H.E., the corresponding current densities are:

3×10^{-4} amp/cm^2 at 1.0 atm Oxygen partial pressure

1×10^{-4} amp/cm^2 at 0.2 atm Oxygen partial pressure

5×10^{-5} amp/cm^2 at 0.1 atm Oxygen partial pressure

The pore can be divided into sections, for example, in three sections as follows:

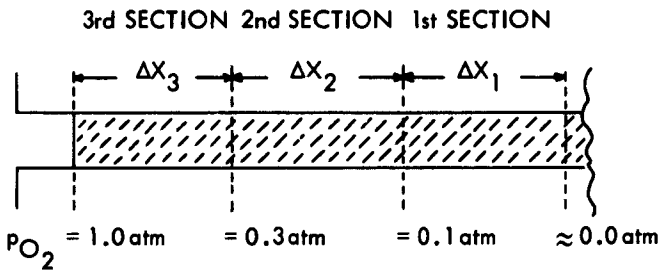

First Section

We can approximate the O_2 concentration as being constant throughout, and equivalent to an oxygen partial pressure of $\frac{0.1 + 0}{2} = 0.05$ atm. Then the surface current density, i_s, will be 2×10^{-5} amp/cm^2. For this section, the length ΔX_1 can be solved for by the approximate relation derived in section 3.1.

$$\Delta X_1 = \left(\frac{2 D_L C_{O_1} Fd}{i_{s1}} \right)^{1/2}$$

$$= \left(\frac{2(1.8 \times 10^{-5})(2.9 \times 10^{-7})(0.05)(96,500)(3 \times 10^{-7})}{2 \times 10^{-5}} \right)^{1/2}$$

$$= 2.74 \times 10^{-5} \text{ cm.}$$

The total number of moles of O_2 flowing into this section will be

$$N_{\Delta X_1} = \frac{i_{s1}(\Delta X_1)\,\pi d}{4F} = \frac{(2\times10^{-5})(2.74\times10^{-5})\,\pi\,3\times10^{-7}}{4(96,500)}$$

$$= 1.34\times10^{-21} \text{ g moles/pore-sec.}$$

Second Section

pO_2 average $= \frac{0.3+0.1}{2} = 0.2$ atm, $i_{s2} = 1\times10^{-4}$ amp/cm^2.

Part of the oxygen will travel through the second section to be reduced in the first section, and we desire to determine the oxygen concentration drop, ΔC_{X_1}, that will be needed in the second section to permit this:

$$N_{\Delta X_1} = 1.34\times10^{-21} = \frac{D_L\left(\Delta C_{X_1}\right)\pi d^2}{\Delta X_2(4)} = \frac{1.8\times10^{-5}\left(\Delta C_{X_1}\right)\pi(3\times10^{-7})^2}{\Delta X_2(4)} \qquad \text{(D-1)}$$

Similarly, as in the first section,

$$\Delta X_2 = \left(\frac{\left(C_{O_2}-\Delta C_{X_1}\right) D_L(2)\,dF}{i_{s2}}\right)^{1/2}$$

$$= \left(\frac{\left(0.2(2.9\times10^{-7}) - \Delta C_{X_1}\right) 1.8\times10^{-5}(2)(3\times10^{-7})\,96,500}{1\times10^{-4}}\right) \qquad \text{(D-2)}$$

From Eqs. D-1 and D-2,

$$\Delta X_2 = 3\times10^{-5} \text{ cm}$$

$$N_{\Delta X_2} = \frac{(3\times10^{-5})(1\times10^{-4})\,\pi\,3\times10^{-7}}{(4)(96,500)} = 7.3\times10^{-21}\ \frac{\text{g moles}}{\text{pore-sec}}$$

Third Section

pO_2 average $= \frac{1.0+0.3}{2} = 0.65$ atm, $i_{s3} = 2.62\times10^{-4}$ amp/cm^2

$$N_{\Delta X_{12}} = N_{\Delta X_1} + N_{\Delta X_2} = (1.34+7.3)\times10^{-21} = 8.64\times10^{-21}\ \frac{\text{g moles}}{\text{pore-sec}}$$

$$N_{\Delta X_{12}} = 8.64\times10^{-21} = \frac{D_L\left(\Delta C_{X_{12}}\right)\pi d^2}{\Delta X_3(4)} = \frac{\Delta C_{X_{12}}}{\Delta X_3}\,1.27\times10^{-18} \qquad \text{(D-3)}$$

Similarly,

$$\Delta X_3 = \left(\frac{\left(C_{O_3} - \Delta C_{X_{12}}\right)(D_L)(2)\ dF}{i_{s3}} \right)^{1/2}$$

$$\Delta X_3 = \left(\frac{\left((0.7)\ 2.9 \times 10^{-7} - \Delta C_{X_{12}}\right)(1.8 \times 10^{-5})(2)\ 3 \times 10^{-7}(96,500)}{2.62 \times 10^{-4}} \right)^{1/2} \qquad \text{(D-4)}$$

From (D-3) and (D-4),

$$\Delta X_3 = 3.86 \times 10^{-5} \text{ cm}$$

$$N_{\Delta X_3} = \frac{(3.86 \times 10^{-4})(2.62 \times 10^{-4})\ \pi\ 3 \times 10^{-7}}{(4)(96,500)}$$

$$= 2.46 \times 10^{-20} \text{ g moles/sec-pore.}$$

The total number of moles of O_2 flowing into the pore will be

$$N_{\Delta X_1} + N_{\Delta X_2} + N_{\Delta X_3} = (2.46 + 0.73 + 0.134) \times 10^{-20}$$

$$= 3.32 \times 10^{-20} \text{ g moles/pore-sec.}$$

The current density per cm^2 of micropore structure will be

$$i_{ps} = \frac{\left(\Sigma N_{\Delta X_i}\right) 4F}{(4)\ d^2} = \frac{3.32 \times 10^{-20}(4)(96,500)}{(4)(3 \times 10^{-7})^2} = 3.56 \times 10^{-2} \text{ A/cm}^2.$$

For other electrode potentials, current-density values can be calculated in a similar fashion.

References

1. L. G. Austin, Paper presented at the Fall Meeting of the American Chemical Society, Chicago, Illinois, 1961.
2. D. Sama, Sc.D. Thesis, Department of Chemical Engineering, M. I. T., 1959.
3. E. Gorin and H. Recht, Chapter 8, Fuel Cells, edited by C. Young (Reinhold Publishing Corporation, New York, 1960).
4. E. Gorin and H. Recht, Ind. Eng. Chem. 52, 301 (1960).
5. G. Gruneberg, Dissertation, Braunschweig Technische Hochschule, July 1958.
6. A. Winsel, Dissertation, Carolo Wilhelmina Technische Hochschule, Braunschweig, January 1957.
7. E. Yeager, The Oxygen Electrode in Aqueous Fuel Cells, Technical Report No. 12, Office of Naval Research Contract Nonr 2391(00), Project NR-359-277 (1960).
8. D. I. G. Ives and G. I. Janz, Reference Electrodes (Academic Press, Inc., New York, 1961).
9. F. Haber, Z. Elektrochem. 12, 415 (1906).
10. F. Haber, Z. Anorg. Allegem. Chem. 51, 245-289 (1906).
11. W. Grube, Z. Elektrochem. 12, 415 (1906).
12. S. Hoar, Proc. Roy. Soc. (London) A142, 628 (1933).
13. J. O'M. Bockris and S. Huq, Proc. Roy. Soc. (London) A237, 277 (1956).
14. W. G. Berl, Trans. Electrochem. Soc. 83, 253 (1943).
15. M. O. Davies, M. Clark, E. Yeager, and F. Hovorka, J. Electrochem. Soc. 106, 56 (1959).
16. R. S. Weisz and S. S. Jaffe, Trans. Electrochem. Soc. 93, 128-141 (1948).
17. D. Sawyer and L. Interrante, J. Electroanal. Chem. 2, 310-327 (1961).
18. R. Lingane, J. Electroanal. Chem. 2, 296-309 (1961).
19. G. Bianchi, G. Caproglio, F. Mazza, and T. Mussini, Chim. Ind. 43, 867 (1961).
20. J. Tafel, Z. Physik Chem. 54, 641 (1905).
21. J. O'M. Bockris and B. E. Conway, Trans. Faraday Soc. 45, 989 (1949).
22. S. Schuldinger and J. P. Hoare, J. Phys. Chem. 61, 705 (1957).
23. S. Schuldinger and J. P. Hoare, J. Phys. Chem. 62, 229 (1958).
24. M. Oikawa, Bull. Chem. Soc. Japan 28, 626 (1955).
25. A. H. Cosjin, J. Electroanal. Chem. 2, 437 (1961).
26. A. H. Cosjin, J. Electroanal. Chem. 3, 24 (1962).
27. N. Hackerman and R. Brodd, J. Electrochem. Soc. 104, 704 (1957).
28. N. Hackerman and J. J. McMullen, J. Electrochem. Soc. 106, 341 (1959).
29. A. Frumkin, Colloid Symposium Anal. 7, 89 (1930).
30. E. W. Thiele, Ind. Eng. Chem. 31, 916 (1939).
31. J. Becker, Trans. Am. Electrochem. Soc. 55, 153 (1929).
32. Ya. Zeldovich, Acta Physicochim. U. R. S. S. 1, 449 (1934); S. Roginski and Ya. Zeldovich, Acta Physicochim. U. R. S. S. 1, 554-595 (1934).

33. W. McAdams, Heat Transmission (McGraw-Hill Book Company, Inc., New York, 3rd edition, 1954).

34. I. Higuchi, T. Ree, and H. Eyring, J. Am. Chem. Soc. 77, 4969 (1955); 79, 1330 (1957).

35. W. M. Kays and A. L. London, Compact Heat Exchangers (McGraw-Hill Book Company, Inc., New York, 1958).

36. C. N. Satterfield and P. Sarda, Rates of Catalytic Decomposition of Liquid Hydrogen Peroxide on Metal Surfaces, Report No. 58, Office of Naval Research, Contract Nonr 1841(11), Project NR-092-008 (1960).

37. K. Kordesh, Chapter 2, Fuel Cells, edited by C. Young (Reinhold Publishing Corporation, New York, 1960).

38. J. Harned, Am. Chem. Soc. 59, 496 (1937).

39. K. Kordesh, U. S. Patent 2,615,932.

40. K. Kordesh, U. S. Patent 2,669,598.

41. International Critical Tables, Vol. VI (McGraw-Hill Book Company, Inc., New York, 1925).

Aeronautical Systems Division, Dir/Aeromechanics, Flight Accessories Lab, Wright-Patterson AFB, Ohio. Rpt No. ASD-TDR-63-118. RATE-LIMITING STEPS ON FUEL-CELL ELECTRODES. Final report, Jan 63, 84p. incl 33 illus., 41 refs.

Unclassified Report

The purpose of this investigation was to identify and to study the step or steps that limit fuel-cell electrode performance. The electrodes considered were the typical porous, gaseous-diffusion type, and most of the effort was directed toward acquiring a more quantitative understanding of the effect of the different variables governing electrode performance. Since it is necessary to be able to predict quantitatively both the mass transfer and the kinetic limitations in order to calculate electrode performances, an experimental program directed to-

(over)

ward obtaining the necessary kinetic data for systems of interest was undertaken. An experimental system was devised by means of which the electrochemical kinetics could be studied over a wide current-density range independently of mass-transfer effects, on electrodes of known catalyst area. In the operating region where the effect of mass transfer became significant, it was possible quantitatively to assess its importance. Electrode-performance calculations were made for the case of an oxygen electrode of idealized geometry, using the experimentally obtained kinetic data and the known values of oxygen solubilities and diffusivities in liquid electrolytes. It was found that if the electrode geometrical parameters (pore-size distribution, location, etc.) are properly chosen, electrode performances much superior to the ones thus far obtained by several investigators should be possible, showing that the potential performance of such types of electrodes has not yet been fully realized.

1. Fuel cells
2. Electrodes
I. AFSC Project 8173, Task 817306
II. Contract AF 33(616)-7624
III. Massachusetts Institute of Technology. Research Laboratory of Electronics. Cambridge, Mass.
IV. Adrian R. Roti
V. Aval fr OTS
VI. In ASTIA collection

Aeronautical Systems Division, Dir/Aeromechanics, Flight Accessories Lab, Wright-Patterson AFB, Ohio. Rpt No. ASD-TDR-63-118. RATE-LIMITING STEPS ON FUEL-CELL ELECTRODES. Final report, Jan 63, 84p. incl 33 illus., 41 refs.

Unclassified Report

The purpose of this investigation was to identify and to study the step or steps that limit fuel-cell electrode performance. The electrodes considered were the typical porous, gaseous-diffusion type, and most of the effort was directed toward acquiring a more quantitative understanding of the effect of the different variables governing electrode performance. Since it is necessary to be able to predict quantitatively both the mass transfer and the kinetic limitations in order to calculate electrode performances, an experimental program directed to-

(over)

ward obtaining the necessary kinetic data for systems of interest was undertaken. An experimental system was devised by means of which the electrochemical kinetics could be studied over a wide current-density range independently of mass-transfer effects, on electrodes of known catalyst area. In the operating region where the effect of mass transfer became significant, it was possible quantitatively to assess its importance. Electrode-performance calculations were made for the case of an oxygen electrode of idealized geometry, using the experimentally obtained kinetic data and the known values of oxygen solubilities and diffusivities in liquid electrolytes. It was found that if the electrode geometrical parameters (pore-size distribution, location, etc.) are properly chosen, electrode performances much superior to the ones thus far obtained by several investigators should be possible, showing that the potential performance of such types of electrodes has not yet been fully realized.

1. Fuel cells
2. Electrodes
I. AFSC Project 8173, Task 817306
II. Contract AF 33(616)-7624
III. Massachusetts Institute of Technology. Research Laboratory of Electronics. Cambridge, Mass.
IV. Adrian R. Roti
V. Aval fr OTS
VI. In ASTIA collection

Aeronautical Systems Division, Dir/Aeromechanics, Flight Accessories Lab, Wright-Patterson AFB, Ohio. Rpt No. ASD-TDR-63-118. RATE-LIMITING STEPS ON FUEL-CELL ELECTRODES. Final report, Jan 63, 84p. incl 33 illus., 41 refs.

Unclassified Report

The purpose of this investigation was to identify and to study the step or steps that limit fuel-cell electrode performance. The electrodes considered were the typical porous, gaseous-diffusion type, and most of the effort was directed toward acquiring a more quantitative understanding of the effect of the different variables governing electrode performance. Since it is necessary to be able to predict quantitatively both the mass transfer and the kinetic limitations in order to calculate electrode performances, an experimental program directed to-

(over)

ward obtaining the necessary kinetic data for systems of interest was undertaken. An experimental system was devised by means of which the electrochemical kinetics could be studied over a wide current-density range independently of mass-transfer effects, on electrodes of known catalyst area. In the operating region where the effect of mass transfer became significant, it was possible quantitatively to assess its importance. Electrode-performance calculations were made for the case of an oxygen electrode of idealized geometry, using the experimentally obtained kinetic data and the known values of oxygen solubilities and diffusivities in liquid electrolytes. It was found that if the electrode geometrical parameters (pore-size distribution, location, etc.) are properly chosen, electrode performances much superior to the ones thus far obtained by several investigators should be possible, showing that the potential performance of such types of electrodes has not yet been fully realized.

1. Fuel cells
2. Electrodes
I. AFSC Project 8173, Task 817306
II. Contract AF 33(616)-7624
III. Massachusetts Institute of Technology. Research Laboratory of Electronics. Cambridge, Mass.
IV. Adrian R. Roti
V. Aval fr OTS
VI. In ASTIA collection

Aeronautical Systems Division, Dir/Aeromechanics, Flight Accessories Lab, Wright-Patterson AFB, Ohio. Rpt No. ASD-TDR-63-118. RATE-LIMITING STEPS ON FUEL-CELL ELECTRODES. Final report, Jan 63, 84p. incl 33 illus., 41 refs.

Unclassified Report

The purpose of this investigation was to identify and to study the step or steps that limit fuel-cell electrode performance. The electrodes considered were the typical porous, gaseous-diffusion type, and most of the effort was directed toward acquiring a more quantitative understanding of the effect of the different variables governing electrode performance. Since it is necessary to be able to predict quantitatively both the mass transfer and the kinetic limitations in order to calculate electrode performances, an experimental program directed to-

(over)

ward obtaining the necessary kinetic data for systems of interest was undertaken. An experimental system was devised by means of which the electrochemical kinetics could be studied over a wide current-density range independently of mass-transfer effects, on electrodes of known catalyst area. In the operating region where the effect of mass transfer became significant, it was possible quantitatively to assess its importance. Electrode-performance calculations were made for the case of an oxygen electrode of idealized geometry, using the experimentally obtained kinetic data and the known values of oxygen solubilities and diffusivities in liquid electrolytes. It was found that if the electrode geometrical parameters (pore-size distribution, location, etc.) are properly chosen, electrode performances much superior to the ones thus far obtained by several investigators should be possible, showing that the potential performance of such types of electrodes has not yet been fully realized.

1. Fuel cells
2. Electrodes
I. AFSC Project 8173, Task 817306
II. Contract AF 33(616)-7624
III. Massachusetts Institute of Technology. Research Laboratory of Electronics. Cambridge, Mass.
IV. Adrian R. Roti
V. Aval fr OTS
VI. In ASTIA collection